Requirements Baseline Document

Technical Note

ESA project METHANE+ led by SRON

Task 1, WP 1000, Deliverable 1 (D1)

Lead author:
Michael Buchwitz (IUP-UB)
Co-authors:
Ilse Aben (SRON), Alba Lorente (SRON), Jochen Landgraf (SRON),
Sander Houweling (VU), Oliver Schneising (IUP-UB), Julia, Marshall (MPI-BGC),
Tonatiuh Guillermo Nuñez Ramirez (MPI-BGC), Cyril Crevoisier (LMD),
Nicolas Meilhac (LMD), Richard Siddans (RAL)

Change log

Version	Date	Status	Authors	Reason for change
1	15-April-2020	Submitted	All (see title page)	New document
1.1	10-June-2020	Submitted	-“-	To consider comments from ESA

Authors

Institute of Environmental Physics (IUP), University of Bremen (UB), Bremen, Germany:

- Michael Buchwitz
- Oliver Schneising

SRON Netherlands Institute for Space Research, Utrecht, The Netherlands:

- Ilse Aben
- Alba Lorente
- Jochen Landgraf

Max Planck Institute for Biogeochemistry (MPI-BGC), Jena, Germany:

- Julia Marshall
- Tonatiuh Guillermo Nuñez Ramirez

Laboratoire de Météorologie Dynamique (LMD), Palaiseau, France:

- Cyril Crevoisier
- Nicolas Meilhac

Rutherford Appleton Laboratory (RAL), UK

- Richard Siddans

Vrije Universiteit Amsterdam (VU), Amsterdam, The Netherlands:

- Sander Houweling

Table of Contents

1. Executive summary

Methane is an important atmospheric greenhouse gas (GHG) and increasing atmospheric concentrations contribute to global warming. Methane plays also an important role in atmospheric chemistry. The atmospheric concentrations of methane need to be carefully monitored and our knowledge about the various natural and anthropogenic sources needs to be improved. Satellite observations of atmospheric methane permit monitoring and help to reduce knowledge gaps with respect to the methane sources and sinks.

This document is a deliverables of ESA project METHANE+, which is led by SRON, The Netherlands. The purpose of this document is to describe the scientific requirements as relevant for this project.

This study intends to contribute to development of the space segment of the global methane monitoring system by building the critical components needed to make optimal use of available instruments, data and tools. Given the identified opportunities and challenges of the current generation of space borne methane sensors, and the scope of the current study, the specific study objectives are as follows:

- Providing support for the algorithm development for the SWIR retrieval from TROPOMI and joint SWIR-TIR retrieval from TROPOMI and IASI/CrIS.
- Assess the quality of the TROPOMI, IASI and CrIS XCH_4 retrievals by comparing data products generated with specific algorithms and product validation using independent ground-based and other data.
- To investigate the added value of combining SWIR and TIR in regional case studies.
- To infer global sources and sinks of CH_4 from inverse modelling of 2 years of TROPOMI and IASI (and/or CrIS) data.
- To investigate the added value of the combined use of SWIR and TIR.
- To investigate the consistency of the SWIR and TIR retrieval datasets, with model simulated transport and chemistry.
- To formulate a road map for future CH_4 remote sensing based on the outcomes of this study as well as parallel studies covering the use of methane from TROPOMI across the full range of scales.

This document is one of the first deliverables of this project and will contribute to the consolidation of the scientific requirements as relevant for this study. To achieve this, the following aspect are addressed in this document:

- A review of the current state of the art w.r.t. satellite instruments, methane retrieval algorithms and related data sets and methane flux inverse modelling tools is presented.
- Validation data sets for the validation of the satellite data products are described.

- An overview about ongoing activities and related projects is given.
- Our current knowledge w.r.t. methane is shortly described and important science questions are presented, which will be addressed in this study.

To achieve the study objectives a number of target regions have to be identified and in this document initial lists are presented. This cover aspects such as (i) target regions, which are considered challenging for the retrievals and (ii) regions and cases which are of interest because of the atmospheric methane signal. Addressing aspect (i) will comprise detailed comparisons of the satellite methane retrievals with the goal to identify retrieval algorithm issues and if possible to solve them. Addressing aspect (ii) primarily requires inverse modelling and related activities.

All these aspects will be covered in this study and the outcome will be documented in separate technical reports.

2. Introduction

Importance of monitoring CH4

The public debate about climate change and the need for mitigating greenhouse gas emissions mostly concerns CO_2. Yet non-CO_2 greenhouse gases contribute close to 80% of the forcing due to CO_2 **/IPCC, 2013/.** Therefore, to limit climate warming to 1.5ºC by the end of the century, important reductions in non-co_2 greenhouse gases will be required **/IPCC, 2018/.** CH_4 accounts for the majority of the climate forcing due to non-co_2 greenhouse gases. In the short term, climate benefits of mitigating CH4 emissions are particularly large due to its limited lifetime. This in combination with the economic co-benefits of several mitigation measures for methane such as preventing unintended methane leakages from the oil and gas sector, make it an attractive target for climate change mitigation policy **/Shindel et al, 2017/.**

Unlike CO_2, anthropogenic emission inventories for CH_4 are associated with large uncertainties. Because of this, inverse modelling methods have been developed to test and improve emission inventories using atmospheric data. The same techniques are applied to CO_2, mostly to address natural fluxes. The UNFCCC supports the verification of national inventory reports using atmospheric data, which Switzerland and the UK have starting doing in recent years for methane **/NIR-UK, 2019; NIR-CH, 2019/**. Currently these efforts are limited to the use of surface measurements. Meanwhile, international space agencies are preparing for the space segment of the global greenhouse gas monitoring system to further support emission verification using atmospheric data.

Within Europe, the Copernicus CO_2 monitoring constellation (CO2-M) is under development. It is focused primarily on CO_2 **/Pinty et al, 2017/,** although extension to CH_4 is being considered as a relatively low cost extension to the mission. Other methane missions already in orbit (GOSAT, TROPOMI) are being used to develop methodology to exploit the specific strengths of satellite remote sensing, i.e. global measurement coverage and the imaging of emission signals at local to regional scales.

To understand the global growth rate of methane, which ultimately determines its radiative forcing, also requires improved information on the natural cycle of methane, including its chemical turnover in the atmosphere.

The natural sources and sinks of methane are themselves driven by processes that are influenced by climatic variations and trends in ways that are still poorly understood.

The global growth rate of methane in the atmosphere shows large fluctuations, the explanation of which has been a major source of controversy in the scientific

literature **/see e.g. Worden et al, 2017/.** The renewed methane increase after 2007 has been attributed to either natural or anthropogenic sources, with the latter dominated either by agricultural or fossil emissions. Last but not least, interannual variability in the hydroxyl radical, the main atmospheric sink of methane, was proposed as the dominant driver of the temporary pause in the methane increase prior to 2007 **/Rigby et al, 2017/.**

This example not only demonstrates the need for atmospheric monitoring of methane, but also that the current capabilities of the monitoring system are still insufficient to provide conclusive answers about its global drivers. At the heart of this problem is the difficulty in separating the various source contributions to the observed methane mixing ratio. As will be explained further below, the solution to this global problem requires resolving the 3D distribution of methane at high resolution, extending the range of relevant scales to be addressed by satellite remote sensing from global to local.

Opportunities and challenges for satellite remote sensing

Past missions (SCIAMACHY, GOSAT) demonstrated the utility of satellites for quantifying methane emissions **/Bergamaschi et al, 2013; Alexe et a, 2015/.** Most studies focused on regional to global scales **/e.g. Cressot et al, 2014; Feng et al, 2017; Pandey et al, 2017; Turner et al, 2016/,** whereas some others also explored the potential of detecting and quantifying signals of local sources ***/Kort et al, 2014; Buchwitz et al, 2017/***. With TROPOMI a wealth of new data is becoming available to continue this development, which the scientific community has only just started to exploit. The major advance that TROPOMI offers for CH_4 comes through the -for CH_4- unprecedented combination of daily global coverage with high spatial resolution (~7x7 km^2) **/Veefkind et al., 2012/.** However, the use of TROPOMI poses new challenges in data processing, including important methodological hurdles that remain to be overcome, in order to optimally benefit from the new data that are becoming available, among which:

- The retrieval of XCH_4 at the high accuracy needed to interpret small signals from local and regional emissions
- Mitigating the impact of transport model uncertainties, with the performance at different scales limited by different processes.
- Resolving mixing ratio gradients, in model and measurements, at the scales needed for process attribution.

Surface measurements, including ground based Fourier Transform Spectrometers, as well as aircrafts have been used to detect and quantify many different anthropogenic sources of methane, including coal mines **/Mackenzie et al, 2017/**, oil & gas production sites **/Karion et al, 2015/**, landfills **/Krautwurst et al, 2017/**, and cattle sheds **/Viatte et al, 2017/**. The measurements have been used to develop techniques for quantifying methane emissions from observed plumes of methane

/Varon et al, 2018/. In several cases the emission source strengths that are reported are within reach of TROPOMI, either from instantaneous overpasses or after averaging.

However, with accuracies of less than 1% (17 ppb) required for total column measurements of CH_4, many sources of error may become large enough to complicate the interpretation of the data. Although the latest operational TROPOMI XCH_4 data product released in March 2019 is already of good enough quality to use **/Hu et al., 2018/,** the algorithms for XCH_4 retrieval at 2.3 micron can still be further optimized. A few issues have been identified in the XCH_4 TROPOMI data **/READMe file/**, such as biases at low surface albedo, which is being further looked into by the SRON team working on the (beta version of the) operational code. Comparison with alternative algorithms -as provided by IUP Bremen in this project- and independent data (TCCON, Aircore, GOSAT) will be a critical means to improve on the TROPOMI S5P XCH_4 data product.

To strengthen the constraint of the TROPOMI data on methane emissions, an alternative to improving measurement accuracy is to further improve the sensitivity of the measurements to the planetary boundary layer where the signals of CH_4 emissions are largest. Surface layer sensitivity is a common argument to prefer sensors operating in the Short Wave Infrared (like GOSAT, TROPOMI) to those operating in the Thermal Infrared (IASI, CrIS). However, the combination of the two has the potential to improve surface sensitivity beyond what is feasible using either instrument type alone **/Worden et al, 2015; Jacob et al, 2016/**, and is one of the objectives of this project.

To attribute inverse modelling estimated fluxes to specific processes requires sufficient spatial resolution to identify the origin, for instance, of large local emissions. Extended identification beyond the footprint size of TROPOMI ($7x7km^2$ in nadir) can be achieved by combining the strengths of TROPOMI (high measurement cover and sensitivity) to that of GHG-SAT (excellent spatial resolution, very limited coverage). An important challenge in methane inverse modelling is to separate its sources and sinks. In global inverse modelling, variation in the chemical sink of methane through reaction with hydroxyl (OH) is estimated from measurements of methyl chloroform **/Montzka et al, 2011; Bousquet et al, 2011/,** or -as in most cases- not optimized at all. Because of the phasing out of methylchloroform (MCF) production to help restore the ozone layer, its mixing ratios will soon become either too low to measure or too uncertain to use **/Liang et al, 2017/**. As an alternative to employing the less powerfull HCFC replacements that have been proposed, the combined use of SWIR and TIR CH_4 retrieval may provide the information needed to separate the signature of sources and OH sink. The former decreases with increasing horizontal and vertical distance from the source whereas the latter increases **/Zhang et al, 2018/**. Besides resolving a lower tropospheric layer by combining SWIR and TIR, TIR measurements provide improved coverage over the ocean compared to SWIR observations which are limited to sunglint geometry over oceans due to the very low surface reflectivity.

Transport model uncertainties pose another important challenge towards improving satellite-supported emission quantification. Local, high resolution, applications of inverse modelling are limited mostly by the ability of models to reproduce the local wind speed and direction. At the global scale, however, the influence of uncertainties in stratosphere – troposphere exchange dominates **/Houweling et al., 2017/**. The combined use of SWIR and TIR allows separating the stratospheric and tropospheric sub-columns. Use of the latter should not only improve the sensitivity to surface emissions, but also has the potential to reduce sensitivity to the uncertainty in the modelled stratosphere-troposphere exchange **/Jacob et al, 2016/**.

In summary the combined use of SWIR and TIR has the following three advantages:

1) Specific information is obtained about the lower tropospheric layer, increasing near-surface sensitivity beyond what is feasible using SWIR only
2) The use of height-resolved information limits the sensitivity of inversions to uncertainties in the modelled strat-trop exchange and other transport processes
3) Vertical profile information and extended coverage of regions at distance from the source (e.g. remote oceans) supports separating the contributions of sources and sinks.

Besides efforts to further develop and test SWIR and TIR retrieval algorithms to further improve the CH_4 satellite products, this project aims to assess the benefits of using the CH_4 observations in these different wavelength ranges concerning these 3 topics. The overall aim is to improve the interpretation of CH_4 satellite data e.g. in terms of quantification of sources and sinks, their spatial distribution and evolution, and their effect on the (evolution of the) regional and global CH_4 budget.

3. Review of current state of the art

This section described the state of the art w.r.t. satellite instruments, retrieval algorithms and related data sets and methane inverse modelling tools.

3.1. Overview satellite instruments

This section presents a short overview about the satellite instruments as used in this study.

3.1.1. TROPOMI/S5P

TROPOMI is the single payload instrument on ESA's Sentinel-5 Precursor mission which was launched on 13 Oct. 2017 **/Veefkind et al., 2012/**. The instrument is jointly developed by the Netherlands and ESA. It is a pushbroom UV-VIS-NIR-SWIR spectrometer which allows to measure many atmospheric constituents such as ozone, nitrogen dioxide, carbon monoxide, sulfur dioxide, methane, formaldehyde etc. The instrument has heritage from earlier European instruments GOME, SCIAMACHY and OMI. TROPOMI has the unique capability to combine high spatial resolution observations with daily global coverage due to its large swath of 2600 km. Individual observations of methane cover an area of 7 x 7 km^2 in nadir, and since 6 Aug 2019 the resolution is even further improved to 7 x 5.6 km^2 (across x along track).

For methane the relevant spectral bands from TROPOMI are the NIR band-6 (around 760 nm) and the SWIR bands 7 and 8 from 2305-2385 nm.
S5P flies in loose formation with Suomi NPP such that the TROPOMI methane retrieval can use the high spatial resolution cloud observations from VIIRS to select cloud-free scenes. With an equator crossing time of 13:30 pm (ascending node), S5P flies a few minutes behind Suomi NPP.

More information on TROPOMI and the status of its measurements and data products can be found on www.tropomi.eu.

3.1.2. IASI

The Infrared Atmospheric Sounding Interferometer (IASI) is a high resolution Fourier Transform Spectrometer based on a Michelson Interferometer coupled to an integrated imaging system that measures infrared radiation emitted from the Earth (https://iasi.cnes.fr/en/IASI/index.htm). Developed by the Center National d'Etudes Spatiales (CNES) in collaboration with the European Organization for the Exploitation of Meteorological Satellites (EUMETSAT), IASI was launched in October 2006 onboard the polar orbiting Metop-A, in September 2012 onboard Metop-B, and in

October 2018 onboard Metop-C. The time series of geophysical variables derived from IASI observations will cover about 20 years.

IASI provides 8461 spectral samples, ranging from 645 cm^{-1} to 2760 cm^{-1} (15.5 µm and 3.6 µm), with a spectral sampling of 0.25 cm^{-1}, and a spectral resolution of 0.5 cm^{-1} after apodization (level1c data). IASI is an across track scanning system, whose swath width is of 2200 km (**Figure 1**), allowing global coverage twice a day. The IFOV is sampled by 2×2 circular pixels whose ground resolution is 12 km at nadir at 9:30 am/pm local time. The combined use of Metop-A and B or Metop-C and B satellites, which are flying on the same orbit but with nearly half an orbit out of phase, yields a complete coverage of the Earth in one day.

The comparison between the 3 IASI at level1 shows that the three instruments agree at the level of 0.1 K or less for the most of the spectrum, and especially in the methane absorption bands at 7.7. µm which are of prime interest for this study.

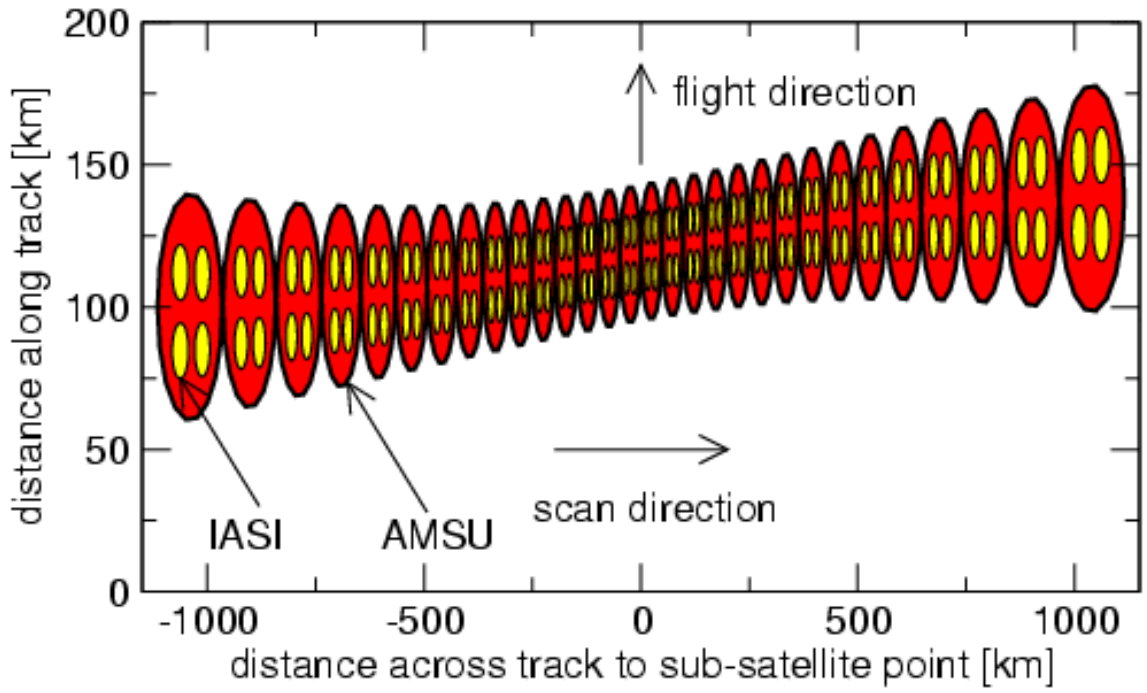

Figure 1: IASI and AMSU scanning geometry (from **/IASI Level 1 Product Guide/**).

3.1.3. CrIS

The Cross-track Infrared Sounder (CrIS) **/Han et al., 2013/** is a TIR spectrometer analogous to IASI flying on Suomi-NPP platform, which is in close tandem orbit with S5P. Within the METHANE+ product the RAL IASI IMS and methane schemes will also be applied to the CrIS TIR spectrometer, enable joint retrievals from precisely co-located TIR/SWIR observations. CrIS data is available since January 2012, however initially in a “nominal” mode in which the spectral resolution was deliberately degraded in the mid and short-wave spectral ranges. Operation in of full spectral resolution (FSR) mode started on November 2 data. FSR L1 data have 2,223 channels: 637 shortwave channels from 3.9 to 4.7 microns (2555 to 2150 cm-1), 869 midwave channels from 5.7 to 8.05 microns (1752.5 to 1242.5 cm-1), and 717 longwave channels from 9.1 to 15.41 microns (1096.25 to 648.75 cm-1). Each CrIS field-of-regard (FOR, ~50x50km at nadir) contains 9 (~12km diameter) field-of-views (FOVs) arranged in a 3X3 array. (I.e. the FOR are similar to IASI, but CrIS obtains 9 observations within each compared to 4 for IASI.)

Also on Suomi-NPP is the Advanced Technology Microwave Sounder (ATMS) **/Han et al., 2019/**. This provides observations analogous to Metop AMSU and MHS, used by the RAL “IMS” scheme. The instrument is a cross-track scanner with 22 microwave channels in the range 23.8-183.31 Gigahertz (GHz). The beam width is 1.1 degrees for the channels in the 160-183 GHz range, 2.2 degrees for the 80 GHz and 50-60 GHz channels, and 5.2 degrees for the 23.8 and 31.4 GHz channels. Since the SNPP satellite is orbiting at an altitude of about 830 km, the instantaneous spatial resolution on the ground at nadir is about 16 km, 32 km, or 75 km depending upon the channel. There are 96 samples in the cross-track direction.

3.2. Overview retrieval algorithms and related data sets

In the following a short overview about the satellite methane retrieval algorithms as used in this study is presented and about the methane data which have been generated with them.

3.2.1. Operational S5P XCH_4 RemoTeC algorithm

RemoTeC is a remote sensing software tool to infer greenhouse gas total column concentrations from shortwave infrared radiance spectra observed by a space borne spectrometer. The software comprises an instrument independent software library, which is utilized by an instrument specific implementation. The software has been applied successfully to GOSAT, OCO-2 and S5P data and is the baseline for CH_4 operational data processing of the S5P and Sentinel-5 mission. The algorithm is described in detail in the literature (e.g. **/Hasekamp et al, 2019/, /Butz et al., 2011/ and /Butz et al., 2012/, /Hu et al, 2018/**] and so, only a short summary will be given here:

Estimating the CO_2, CH_4 and/or H_2O total column concentrations from shortwave infrared measurements faces the challenge that the light-path from the sun to the satellite observer via backscattering at the Earth's surface is not known with sufficient accuracy. In practice, light scattering by atmospheric particles causes unknown light path modification. As a consequence, state-of-the-art retrieval algorithms must retrieve particle properties simultaneously with the CO_2, CH_4, and H_2O concentration. Therefore, RemoTeC aims at retrieving the trace gas vertical profile (with slightly more than 1 degree of freedom) and 3 scattering parameters characterizing the particle amount, size and height. Particle amount is represented through the total column number density of particles. For the particle number density size distribution, RemoTeC assumes a power-law $n(r) \sim r^{\alpha}$, with r the particle radius and α the retrieved size distribution parameter. The particle height distribution is a Gaussian function of center height z_c and a fixed width of 2 km. Particle refractive index (m_r, m_i) is assumed to have a fixed value, $m_r = 1.400$ and $m_i = -0.003$. The retrieval method infers the partial column concentration profile, the three aforementioned particle parameters, interfering absorber concentrations as well as some auxiliary parameters such as surface albedo by iteratively minimizing the Phillips-Tikhonov cost function. The software is thread safe and managed under version control and thus well suited for the purpose of this project.

Note: The version of the RemoTeC algorithm is the same as the one used to generate operational S5P-CH4 product, but with different settings (beta version (or scientific version) of the operational retrieval algorithm).

3.2.2. Scientific S5P XCH_4 WFMD algorithm

The scientific retrieval algorithm WFMD (or WFM-DOAS, Weighting Function Modified Differential Optical Absorption Spectroscopy) for the retrieval of methane and carbon monoxide from the spectral radiances as measured by the TROPOMI instrument onboard the Sentinel-5 Precursor (S5P) satellite is described in detail in **/Schneising et al., 2019a, 2019b/**.

In short, WFMD is a linear least-squares method based on scaling (or shifting) pre-selected atmospheric vertical profiles. The vertical columns of the desired gases are determined from the measured sun-normalised radiance by fitting a linearized radiative transfer (RT) forward model to it.

The RT forward model is derived from the radiative transfer model SCIATRAN **/Rozanov et al., 2002, 2014/** in pseudo-spherical atmosphere mode. Spectroscopic line parameters are from **/HITRAN2016/**. To enable a fast retrieval, a look-up table scheme for the radiances and their derivatives has been implemented containing 17280 reference spectra for varying solar zenith angle, altitude, albedo, water vapour, and temperature. The reference spectra are computed with high spectral resolution in line-by-line mode and subsequently convolved to TROPOMI spectral resolution of the SWIR bands using an instrument specific fixed spectral response function extracted from the TROPOMI ISRF Calibration Key Data v1.0.0 for nadir at 2338 nm.

The linearized radiative transfer model (appropriately chosen from the look-up table according to the relevant parameters) plus a low order polynomial is linear least squares fitted to the logarithm of the measured sun-normalised radiance. The trace gas vertical profiles (CH_4, CO, H_2O) are scaled for the fit (i.e., the profile shape is not varied). Additional fit parameters are the shift of a pre-selected temperature profile, a scaling factor for the pressure profile, and parameters for a second order polynomial.

Due to the potential non-linear dependencies of the radiances with respect to water vapour and temperature within their natural variability, the algorithm treats both parameters iteratively. The algorithm starts with look-up table elements representing U.S. Standard Atmosphere water vapour amount and temperature. If the retrieved parameter pair after the fit is closer to another look-up table element, the process is repeated with the corresponding reference spectrum. Usually convergence is achieved after one iteration step.

The spectral fitting windows in TROPOMI band 7 were optimised to retrieve CH_4 and CO simultaneously as accurately as possible (determined by an error analysis based on simulated measurements). Note that CO is a much weaker absorber compared to CH_4 and H_2O. The apparent albedo is retrieved in the pre-

processing by comparison of the measured continuum radiance with pre-calculated values from a look-up table. Cloud information is obtained from strong H_2O absorption lines in S5P band 8 by comparing the measured radiances to reference radiances for cloud-free conditions. As the absorption in these lines is strong, the measured radiance is small in the clear sky case. In the presence of clouds, most of the atmospheric H_2O is shielded and the measured backscattered radiance coherently increases **/Heymann et al., 2012/**. The corresponding ratio of measured to reference radiance for the selected strong absorption lines is thus an indicator of cloud contamination.

In order to convert the retrieved vertical columns into column-averaged dry air mole fractions (denoted XCH_4 and XCO), the columns are divided by the dry air column obtained from the European Centre for Medium-Range Weather Forecasts (ECMWF) analysis. Thereby, the ECMWF dry columns are corrected for the actual surface elevation of the individual TROPOMI measurements (based on the deviation from the mean altitude of the coarser model grid) inheriting the high spatial resolution of the satellite data.

Post-processing includes quality filtering and bias correction, which is achieved via machine learning using Random Forest based methods (see **/Schneising et al., 2019a, 2019b/** for details).

Currently available (i.e., at project start) is a first data set generated with WFMD/S5P version 1.2, which covers the time period November 2017 until end of 2018. This data set is available from: http://www.iup.uni-bremen.de/carbon_ghg/products/tropomi_wfmd/.

An analysis based on simulated measurements suggests that typical systematic retrieval errors after quality filtering are below 1%. The validation with TCCON provides realistic error estimates. The corresponding error characteristics can be summarised as follows:

- Single observation random error: 14 ppb (1-sigma)
- Relative accuracy (spatio-temporal bias): 4.4 ppb

Due to the relatively short time period of the existing WFMD v1.2 data set a long-term bias drift or year-to-year bias variability has not yet been assessed.

3.2.3. IASI NLIS upper tropospheric CH_4 algorithm

Mid-tropospheric columns of methane (CH_4) and carbon dioxide (CO_2) are retrieved from simultaneous observations of the IASI and AMSU instruments flying together onboard the Metop satellites using the non-linear inference scheme (NLIS) developed at CNES-LMD **/Crevoisier et al., 2009a, 2009b, 2013/**. The NLIS algorithm is based on Multi-Layer Perceptrons with 2 hidden layers. IASI hyperspectral observations in the thermal infrared at 7.7 µm (resp. 15 µm), which are sensitive to both temperature and gas concentrations of CH_4 (resp. CO_2) are used in conjunction with microwave observations form the AMSU instruments, only sensitive to temperature, to decorrelate both signals.

Only a subset of IASI channels presenting the best properties with regards to the retrieval performances are used. 24 channels have been selected to optimize the signal-to-interference ratio, in particular to minimize the spectral interference of H_2O, which dominates the infrared spectrum in methane absorption bands. The selected channels are not sensitive to variations of methane in two parts of the atmosphere: the lower troposphere (roughly below 500 hPa) and the tropopause **/Crevoisier et al., 2003/**. The Jacobians of the selected channels have very similar shapes and all peak around 260 hPa. Hence, the NLIS algorithm deliver a mid-tropospheric column of methane.

The neural networks are trained on a learning dataset with couples of known inputs-outputs from the TIGR database and evaluated on an evaluation dataset (ARSA). The retrievals are performed on a global scale during day and night-time (9:30 am/pm local time), both over land and over sea.

The radiative simulations in the thermal infrared used to train the networks are based on the fast and accurate line-by-line radiative transfer model 4A (Automatized Atmospheric Absorption Atlas) ***/Scott and Chédin, 1981/***. 4A is an advanced version of the nominal line-by-line STRANSAC model (Scott, 1974) and is basically a compressed look-up-table of optical depths calculated once and for all. It can be coupled to any spectroscopic databases and can simulate any instrumental configurations (ground, airborne, satellite). In addition to the simulation of atmospheric transmissions and radiance (or equivalently brightness temperature (BT)) spectra, 4A analytically computes Jacobians for all relevant atmospheric variables. 4A is the official code chosen by CNES for calibration/validation and preparation activities of several space missions, including IASI and IASI-NG. For the NLIS algorithm, the spectrometric parameters used as inputs to 4A, are taken form the GEISA-2011 database **/Jacquinet-Husson et al., 2011/**.

Once the learning phase is completed, observations of IASI and AMSU can be used to infer mid-tropospheric columns of CH_4 or CO_2. The retrieval is performed at the AMSU resolution: when 4 IASI FOVs included in 1 AMSU FOV are declared clear

(meaning that no cloud nor aerosol has been detected), the BTs of the channels are averaged over the 4 IASI FOVs and used together with AMSU BTs, to perform the retrieval.

Note: The cloud and aerosol detection is the one that has been developped for IASI processing at LMD since 2007 and described in **/Crevoisier et al., 2009b/** and **/Capelle et al., 2018/**. Main difference with EUMETSAT IASI-L2 cloud product concern low clouds and aerosols that are under-estimated in the official product, yielding regional biases on terms of GHG.

Since the networks are trained with simulated data, potential systematic radiative biases existing between simulations used in the learning phase and observations must be removed before using these BTs as inputs to the network corresponding to the situation according to the scan angle, surface elevation and air-mass type. These systematic radiative biases are computed with the calibration/validation chain that has been developed for many years at LMD ***/Armante et al., 2016/***. For each channel, the differences between simulations and collocated (in time and space) satellite observations are averaged over several full years of operation. These differences are called 'calc-obs' residuals. The simulations are performed using the 4A/OP forward model and radiosonde measurements from ARSA as inputs. Every month, about 100 collocations are available, giving access to robust statistics. Specific radiative biases have to be taken into account for each scan angle. Here we refer to collocations between ARSA atmospheric situations, used as inputs to the LMD 4A radiative transfer code, and IASI/AMSU observations. This is done for each Metop satellite.

Through comparisons with regular aircraft **/Machida et al., 2008/** or balloon **/Membrive et al., 2017/** measurements as well as observations made at the surface, it has been shown that, once the radiometric characterization of the instruments is performed, IASI and AMSU capture well the trend and interannual variation of CH_4, with an excellent agreement with the rate of increase measured at the surface, giving confidence in the ability of IASI to follow its evolution over the 20 years of the Metop program.

3.2.4. RAL algorithms

3.2.4.1. Infra-red Microwave Sounder (IMS) retrieval scheme

The Infrared Microwave Sounding (IMS) scheme **/Siddans, 2019/** employs the optimal estimation method (OEM) to jointly retrieve water vapour, temperature and ozone profiles, surface spectral emissivity and cloud parameters from the Metop sounding instruments IASI, MHS and AMSU. RTTOV is used as the forward model for all three sensors. In the current context, is used to provide input temperature, humidity and surface emissivity information for the RAL methane retrieval scheme (see below). The IMS scheme was developed in the context of a Eumetsat study which started with the specification of the Eumetsat operational optimal estimation scheme used for the version 6 operational product.
During the study three advances over the Eumetsat OEM were developed:

- Information from IASI, AMSU and MHS measurements are combined
- Spectral emissivity is jointly retrieved
- Cloud parameters are included in the retrieval, enabling the scheme to be applied to cloudy scenes without major degradation in the main target variables.

Those three extensions were found to improve agreement with ECMWF analyses of lower tropospheric water vapour and to reduce the sensitivity to small amounts of cloud contamination; significantly improving the coverage of useful data.
The IMS scheme was subsequently developed through work within the UK National Centre for Earth Observation (NCEO). The scheme now uses a weak prior constraint, based on zonal mean climatology. It is in practice therefore independent of ECMWF analyses or re-analyses (except for surface pressure). The IMS scheme uses the RTTOV radiative transfer model to simulate brightness temperature observations of the IASI and microwave sounders.

Via NCEO, the IMS scheme has been applied to process the complete IASI Metop A mission from 2007 to 2016. This “Version-1” dataset is made available in Year-1 to the CCI+ Water Vapour project. The water vapour profiles have been independently validated in this project and shown to improve on the operational product. This data is now archived at CEDA (http://www.ceda.ac.uk/). More recently, the IMS scheme has been developed further, building on new capabilities introduced in RTTOV 12:

- The quality of the height-resolved ozone retrieval has been much improved.
- Joint retrieval of additional trace gases including carbon monoxide (CO), nitric acide (HNO3), methanol (CH3OH), ammonia (NH3) and formic acid (HCOOH).
- Joint retrieval of dust and sulfuric acid aerosol optical depth. The latter is a particularly important additional for methane, as sulfuric acid aerosol has spectral features which interfere to some extent with methane and are

suspected as causing anomalous methane results following strong volcanic eruptions.

- Cloud is now represented as a multiple scattering layer using spectral optical properties of ice / liquid cloud. Effective radius, altitude and optical depth of the cloud are now jointly retrieved.

It is expected to apply the improved IMS scheme to Metop-B to provide the necessary inputs for processing Metop-B with the RAL methane scheme (below). Within this project primarily Metop-B will be used and potentially also CrIS. In the past the IMS scheme has been applied to Metop-A.

3.2.4.2. TIR Methane retrieval scheme

RAL's optimal estimation based IASI methane (CH_4) retrieval scheme provides global height-resolved information on methane from the thermal infrared v_4 methane absorption band in the interval 1232–1288 cm^{-1} **/Siddans et al., 2017/**. In addition to retrieving CH_4 on 12 pressure levels, the processor co-retrieves H_2O (on 16 pressure levels), a scale factor for the HDO/H_2O ratio assumed in HITRAN 2008, a scale factor for $^{13}CH_4$, effective cloud fraction, effective cloud top pressure, surface temperature, and scale factors for two systematic fit residuals. The latest version of the processor uses temperature, water vapour and surface spectral emissivity pre-retrieved by RAL's Infrared Microwave Sounder (IMS) scheme as input, based on collocated measurements from IASI, MHS and AMSU **/Knappett et al., 2018/**.

The processor forward model is based on RTTOV, using in-house coefficients derived for the retrieval window by running the line-by-line Reference Forward Model (RFM) **/Dudhia, 2016/** with spectroscopic line parameters from HITRAN 2008. The CH_4 prior used in the retrieval is based on 2009 output from the chemical transport model TOMCAT and varies latitudinally but not temporally, ensuring that any trend in retrieved CH_4 does not originate from the prior.

Scenes containing thick cloud are screened out of the retrieval at an early stage though a brightness temperature test in the IASI window channel at 950 cm^{-1}. Furthermore, accurately modelling N_2O in the fit window, but excluding N_2O from the state vector, enables the retrieval of effective cloud parameters from N_2O absorption features, which corrects for the effects of optically thin cloud on retrieved CH_4.

RAL IASI CH4 retrievals show good agreement with model data from the MACC greenhouse gas inversion, as well as independent measurements from the SWIR satellite GOSAT and ground-based TCCON network, when based on IASI spectra from both MetOp-A **/Siddans et al., 2017/** and MetOp-B **/Knappett et al., 2018/**.

3.2.4.1. Joint TIR+SWIR methane scheme

In order to obtain specific information on lower tropospheric methane, a combined TIR+SWIR retrieval scheme is being developed by Dr. Knappett at RAL under the ESA Living Planet fellowship project 'PROMCOM' (Jan'19 – Dec'20) co-funded by NCEO. The TIR+SWIR scheme will take the form of either a "L2-L1" combined retrieval, where S5P L2 methane is used to constrain the RAL TIR methane retrieval, or a "L2-L2" combined retrieval, where S5P L2 methane and RAL TIR L2 methane are combined post-retrieval. Initial work with L2-L2 combination based on optimal estimation has been promising and it is expected that this approach will be applied in METHAN+. In principle the scheme can be applied to IASI+S5P or CrIS+S5P, though for IASI some errors due the different sampling times are inevitable. More details on the algorithm will be provided (in the ATBD) after the approach is consolidated via the ongoing work in PROMCOM.

3.3. Overview CH_4 flux inverse modelling tools

3.3.1. TM5-4DVAR (VU)

The following subsections describe the main elements of the TM5-4DVAR inverse modelling system. We make use of the version that is being maintained and developed for the CH_4 inversion reanalysis that is made available by the Copernicus Atmospheric Monitoring Service (CAMS). The description that is provided here is a modified version of the documentation of the CH_4 inversion production chain that is available from the CAMS website **/Segers et al., 2020/**.

3.3.1.1. TM5 Chemistry Transport Model

TM5-4DVAR uses the global atmospheric transport model TM5 **/Huijnen et al., 2010; Krol et al., 2005/**. The offline TM5 model makes use of meteorological inputs from a weather prediction model, for which the ECMWF reanalysis is most commonly used. The standard advection algorithm in TM5 is based on the slopes scheme developed by **/Russell and Lerner, 1981/**. Both deep and shallow cumulus convection is evaluated using the Tiedtke scheme **/Tiedtke et al., 1989/**. When available, ECMWF archived convective mass fluxes are used replacing the online convection calculations. In the free troposphere vertical diffusion is computed based on wind shear and static stability following **/Louis, 1979/**, while in the planetary boundary layer vertical diffusion is parameterized based on the revised LTG (Louis, Tiedtke and Geleyn) scheme of **/Holtslag and Boville, 1993/**. The scheme explicitly accounts for stable conditions in the surface layer based on the Monin-Obukhov similarity theory. The diurnal variation of the boundary layer height is determined following **/Vogelezang and Holtslag, 1996/** from ECMWF surface latent and sensible heat fluxes in combination with the vertical profiles of temperature and humidity. The performance of this combination of turbulent and advective transport parameterizations has been evaluated by **/Peters et al., 2004)/** using sulphur hexafluoride (SF_6) simulations.

The model allows a two-way nesting of regions as described in /**Krol et al. (2005)**/. A grid configuration using zoom regions typically consists of a global domain at $6^o \times 4^o$ or $3^o \times 2^o$ resolution, an intermediate zoom region at higher resolution, and a target zoom region at $1^o \times 1^o$ to $0.5^o \times 0.25^o$ embedded in the intermediate domain. In the polar regions (>80 N/S) the number of grid cells in the longitudinal direction is gradually reduced towards the poles to avoid violation of the Courant-Friedrichs-Lewy (CFL) criterion **/Bregman et al., 2003/**.

In TM5-4DVAR, meteorological inputs are the model from ECMWF, using either the ERA-Interim or ERA5 re-analysis. In ERA-5, which will be used in this study, the resolution of the meteorological data has increased compared to ERA interim from ~60 to ~30 km, and the number of layers has increased from 60 to 137. The input

frequency of the meteorological data is increased to hourly, which is only used for the surface field to limit storage and reading time of 3D fields. In the vertical domain a subset of levels is chosen out of either the standard 60 (ERA-Interim reanalysis) or 137 hybrid sigma-pressure levels (ERA-5). The vertical distribution is chosen such that it covers the full domain of the ECMWF model, i.e. including the middle atmosphere, while having especially good vertical resolution in the planetary boundary layer and in the tropopause region to resolve possibly steep tracer gradients. The model typically uses a configuration with 34 vertical layers.

Mass fluxes are computed as described in **/Segers et al., 2002/**. Most meteorological data are pre-processed and stored at 1°×1°, native vertical resolution, and three-hourly frequency, using either time averaged or hourly interpolated data. The coarsening to the resolution of the TM5 simulation is done on the fly within the TM5 model (or using the model to generate coarsened output). For simulations at a higher spatial resolution (e.g. 0.5°×0.25°), the 1°×1° data can be interpolated. Alternatively, dedicated regional meteorological fields can be created based on high-resolution ECMWF data.

3.3.1.2. 4DVAR Inversion methodology

The inversion system estimates monthly global fields of CH_4 surface fluxes that provide an optimal match between simulated and observed CH_4 concentrations, when prescribed as input to the TM5 model. The various components and configuration of this system are described below, following the standard notation proposed in **/Rayner et al., 2019/** and summarized in Table 1 of that study.

In the inversion system, the optimal state $\boldsymbol{x}$ is defined as the state where the following cost-function reaches a minimum value:

$$J(x) = \frac{1}{2}(x - x_b)^T B^{-1}(x - x_b) + \frac{1}{2}(H(x) - y)^T R^{-1}(H(x) - y) \qquad Eq.1$$

In summary, the cost-function assigns a penalty when $\boldsymbol{x}$ differs from a background state $\boldsymbol{x_b}$, and when the simulation ($\boldsymbol{x}$) differs from the observations $\boldsymbol{y}$. The observation operator $\boldsymbol{H}$ consists of the chemistry-transport model that simulates concentrations given the meteorological information and the state estimate $\boldsymbol{x}$. The background covariance matrix $\boldsymbol{B}$ and the observation error covariance matrix $\boldsymbol{R}$ specify the relative weight of the two penalties in the total sum.

The state $\boldsymbol{x}$ for which Eq.1 reaches the minimum is obtained using the M1QN3 algorithm **/Gilbert and Lemaréchal, 1989/,** based on the the limited memory Broyden-Fletcher-Goldfarb-Shanno (L-BFGS) technique. This iterative procedure converges to the cost function minimum, using typically about 50 iterations. After each iteration an updated state vector estimate is derived using the following:

- the current state estimate $\boldsymbol{x}_i$;
- the evaluated costs $J(\boldsymbol{x}_i)$ for this estimate;
- the cost function gradient $\nabla_x J(\boldsymbol{x}_i)$ with respect to the state vector elements evaluated at the intermediate solution $\boldsymbol{x}_i$.

The iteration step results in a new estimate $\boldsymbol{x}_{i+1}$ of the optimized state. The iteration process is terminated after a convergence criterion is satisfied, defined is a reduction in $\nabla_X J(\boldsymbol{x})$ that has to be achieved, or after a predefined number of iterations has been completed.

The minimization procedure requires evaluation of the gradient of the cost function towards the elements of the state, which is computed using

$$\nabla_x J(x) = B^{-1}(x - x^b) + H^T R^{-1}(H(x) - y) \qquad \textit{Eq. 2}$$

where $\boldsymbol{H}^{\mathrm{T}}$ represents the adjoint observation operator, computed using the adjoint of the chemistry-transport model towards the state variables. The input for the adjoint model is the departure vector:

$$\delta y = R^{-1}(H(x) - y) \qquad \textit{Eq.3}$$

which consists of the differences between observations $\boldsymbol{y}$ and their simulations $\boldsymbol{H}(\boldsymbol{x})$, weighted with the assumed observation error covariance $\boldsymbol{R}$. The inverse of the background covariance $\boldsymbol{B}$ is not explicitly computed. Instead, a pre-conditioner is applied (for details see ***/*Segers et al, 2020*/***).

The background covariance $\boldsymbol{B}$ represents the uncertainty in $\boldsymbol{x}$, i.e. of the CH_4 emissions that are optimized. To reduce the requirements on computer memory, the full $\boldsymbol{B}$ matrix is not computed, but only represented in a parameterized form using a few simplifying assumptions. The uncertainties in the emissions are assumed to be uncorrelated between the four emission processes that are considered (see section 3.3.1.4). The $\boldsymbol{B}$ matrix has therefore a block-diagonal form:

$$B = \begin{pmatrix} B_{e1} & \cdots & 0 \\ \vdots & \ddots & \vdots \\ 0 & \cdots & B_{e4} \end{pmatrix} \qquad \textit{Eq.4}$$

Each of the four diagonal blocks describes the covariance in the monthly time series of 2D emission fields. This covariance is parameterized as the product of a standard deviation and a correlation:

$$B_{ei} = S_{ei} C_{ei} S_{ei} \qquad \textit{Eq.5}$$

where the $\boldsymbol{S}$ matrix is a diagonal matrix representing the standard deviation of the emissions, and the $\boldsymbol{C}$ matrix holds the correlations. A standard deviation of 1.0 (100%) is assumed, except for category 'other' for which a standard deviation of 0.50 (50%) is assumed. The correlations within the time series of emission deviation fields are assumed to be separable in a spatial (horizontal) and temporal component, and can therefore be written as the Kronecker product

$$C_{ei} = C_{ei,h} \otimes C_{ei,t} \qquad \textit{Eq.6}$$

The horizontal correlations are parameterized as being homogeneous (the same everywhere) and isotropic (independent of direction). The correlation between the emission deviations in two grid cells therefore only depends on the distance between the grid cells, assuming a Gaussian decay

$$c_{h;i,j} = exp\left(-\frac{1}{2}\left(\frac{d_{i,j}}{L}\right)^2\right) \qquad \textit{Eq.7}$$

where $d_{i,j}$ is the distance between the centers of cell *i* and *j* in km, and *L* is the correlation length scale, which are in this application 500km for each of the emission categories. For the wetlands, rice, and biomass burning categories, no temporal correlations are prescribed ($\boldsymbol{C}_t = \boldsymbol{I}$). Thus, for these categories large fluctuations in time are allowed, which is in line with the strong seasonal pattern in the corresponding emissions. For category 'other' (mainly anthropogenic), the deviations are assumed to be smoother in time, and therefore a temporal correlation is prescribed with an exponential decay that depends on the distance in months:

$$C_{t;m,n} = exp\left(-\frac{|m-n|}{\tau}\right) \qquad \textit{Eq.8}$$

where *m* and *n* are the month numbers and τ is the temporal correlation scale of 9.5 months.

3.3.1.3. TM5-4DVAR Inversion setup and a prior information

Monthly CH_4 fluxes are estimated for every surface grid box of the model and four different emission categories:

- wetlands;
- rice fields;
- biomass-burning;
- other sources

In the inversion, emission adjustments from the *a priori* or background emission $\boldsymbol{E}^{b}{}_{i,j,t}$ are represented by state vector elements $\gamma i,j,t$ for grid cell (i, j) and time t represent The state vector elements are related to the actual emission $\boldsymbol{E}_{i,j,t}$ as follows

$$E_{i,j,t} = \begin{cases} E^{b}_{i,j,t} exp(\gamma_{i,j,t}), \gamma_{i,j,t} < 0 \\ E^{b}_{i,j,t}(1 + \gamma_{i,j,t}), \gamma_{i,j,t} \geq 0 \end{cases} \qquad Eq.9$$

This *semi-exponential* formulation is needed to ensure that actual emissions are always positive, since nothing prevents $\gamma i,j,t$ to change sign. A priori estimates for the specified categories are composed from different inventories as describe below and summarized in **Table 1**.

Wetland emissions
Wetland emissions are taken from a simulation with LPJ-wsl **/Zhang et al. 2018/**. This set provides emissions for 1990-2017, for earlier years the 1990 simulations are used and for later years the 2017 simulations.

Anthropogenic emissions
Rice fields and the 'other' anthropogenic sources are taken from the EDGAR v4.3 inventory **/Janssens-Maenhout, 2017/**. This inventory provides emissions up to 2012. The inventory consists of gridded maps of yearly total emissions for a number of source categories. Two postprocessing steps are applied to these data:
For years after 2012, an extrapolation in time is made using yearly growth factors that are applied to the gridded fields valid for 2012. The growth factors are based on proxies for global fossil fuel and agricultural production, taken from BP and FAO respectively. If these statistics are not available for the most recent years, a linear extrapolation is used.

For the year 2010, the inventory also includes gridded maps per month. The relative time profile per grid cell for this year is used for all years of the inventory, including the temporal extrapolation for recent years. Note that for rice fields, the time profile provided with the 2010 emissions was found to be incorrect, since it represents the activity of agricultural soil management. Instead, for rice emissions a seasonality is used based on the regionally varying rice cropping season **/Matthews, 1991/**.

Biomass burning
Biomass burning emissions are taken from GFAS **/Kaiser et al., 2012/**, as available from the CAMS fire emission service from 2003 onwards. For the 1990-2002 period the ACCMIP/MACCity inventory is used **/Granier et al., 2011/**.

Table 1: Overview of *a priori* emission inventories used in TM5-4DVAR. The colors represent the different emission super-categories that are optimized by the inversion.

Category	Period	Source
wetlands	*climatology*	Kaplan
rice	1989-2008	EDGAR v4.2 with Matthews seasonality
	2009-2017	EDGAR v4.2 with Matthews seasonality (valid for 2008)
biomass burning	1989-1996	ACCMIP-MACCity
	1997-2011	GFED v3.1
	2012-2017	GFED v3.1 climatology 1997-2010
other anthropogenic	1989-2008	EDGAR v4.2
	2009-2017	EDGAR v4.2 (valid for 2008)
oceans	*climatology*	Lambert
wild animals	*climatology*	Olson
soil sink	*climatology*	Ridgwell
termites	*climatology*	Sanderson

Remaining sources and soil sink
Climatologies are used for the remaining sources (oceans, wild animals, and termites), as well as for the soil sinks.

Atmospheric sinks
For photochemical loss of CH_4, oxidant abundances are computed off-line by full-chemistry transport models. The following datasets are used:

- For the tropospheric sink, loss rates are based on monthly OH fields simulated by the TM5 model, which were further optimized using methyl chloroform measurements **/Bergamaschi et al., 2005; Houweling et al, 1998/**.
- Stratospheric loss rates are computed using OH, Cl, and O(1D) abundances taken from ECHAM5/MESSy1 **/Jöckel et al., 2006/**.

Note on source attribution at regional scale

At the coarse resolution of the global systems that are used, very limited information is obtained to address specific anthropogenic source categories. For this reason TM5-4DVAR does not provide specific estimates for livestock and landfills. It is possible to obtain updated estimates for those sources, by using the a priori source profile to disaggregate the a posteriori total per grid cell. However, so far this has only been used to facilitate the comparison with other inversions that aggregate the source categories in a different manner (e.g. for GCP-CH4).

3.3.1.4. Observations

The observation vector $\boldsymbol{y}$ collects all measured values that should be used to optimize the state. The observations are collected for the time window of the 4D-var optimization, which is here either 24 or 48 months. In this existing application, the observations are ground-based observations from the NOAA network, and satellite column-mean mixing ratios from the GOSAT satellite. The use of TROPOMI data has been initiated as part of H2020 Verify, and will be continued within METHANE+.

Surface observations

Surface observations are available from the NOAA Earth System Research Laboratory (ESRL) global cooperative air sampling network **/Dlugokencky et al., 2009/**. These concern CH_4 dry air mole fractions measured at the surface. The observations are acquired preliminary from the official release through personal communication with the providers, within 2-3 months after observation. The station selection excludes observation sites with significant local influence. In addition, sites are only selected if long time series without significant data gaps are available, to minimize temporal variations in the network geometry.

A pre-processing is applied to the raw data in order to average the samples within 3-hourly windows. Multiple observations at these small temporal scales are present from sites with duplicate sampling or high temporal frequency. For an estimate of the uncertainty, the NOAA product comes with an *analysis error* value; this is currently not used however, and a constant error standard deviation of 3 ppb is assigned to each (averaged) observation.

Surface observations are sampled from TM5 simulated mixing ratios. In the horizontal, the concentrations are interpolated from the model grid to the station location using bi-linear interpolation. In the vertical, the concentrations are interpolated to the altitude of the site (in m above sea level); this is not necessarily the lowest model, since the model orography is at coarse resolution and therefore a smooth version of the true orography. In case the site is located below the model orography (e.g., in a valley), the concentrations at the surface are used.

The observation representation error is computed following **/Bergamaschi et al., 2010/**. The base is the assumed measurement uncertainty of 3 ppb, with additional contributions for the model representation error based on 3-D gradients of simulated CH_4 mixing ratios, local emissions, and boundary layer height development.

Satellite retrievals

From 2009 onwards, satellite observations from GOSAT are available to constrain the surface fluxes too. The total columns XCH_4 from this instrument have been

proven to be a useful source of information on methane concentrations. The inversion setup follows /Pandey et al., 2016/ with respect to the treatment of XCH_4. For the optimization of the CH_4 fluxes, the production chain uses GOSAT XCH_4 columns. The product used is the RemoteC XCH_4 PROXY, as retrieved by SRON for the ESA/CCI project **/Detmers & Hasekamp, 2016/**. The PROXY product is based on the ratio between the CH_4 and CO_2 signal, and assume proper knowledge of the CO_2 field **/Schepers et al., 2012/**. The product includes a bias correction as function of the retrieved albedo, based on comparison of the retrievals with TCCON XCH_4 observations.

In the 4DVAR optimization, TM5 is sampled according to the time and location of each valid GOSAT retrievals, using the corresponding averaging kernel. Following **/Pandey et al., 2016/**, a bias correction is applied to GOSAT XCH_4. The correction is based on a comparison of the TM5 inversion using NOAA surface observations only and the original retrieval product. It accounts for inconsistencies between inversions using in situ and satellite data, caused most likely by a combination of transport model and spectroscopic uncertainties. The current bias correction is computed per month and per latitude band of 5 degrees. At Antarctic latitudes the bias is strongly positive and is rather scattered; for this, all GOSAT retrievals below 60^oS are ignored (at high latitudes, large residuals are found between TM5 and GOSAT, in part because retrieval uncertainties increase, in part because of inaccuracies in the representation of CH_4 in the polar vortex in TM5).

Note on use of TROPOMI data in VERIFY

Within VERIFY TROPOMI data have been integrated in TM5-4DVAR, comparisons are being made with the CAMS inversion using surface or GOSAT data and a bias correction has been developed following the same methodology as has been used for GOSAT in the past.

Note on Fluxnet

Fluxnet is not being used, because the data are poorly representative of the spatial scales that are resolved by the global inversion.

3.3.2. Jena CarboScope (MPI-BGC)

3.3.2.1. TM3 Chemistry Transport Model

The Tracer Model TM3 is a global, three-dimensional atmospheric chemistry transport model (CTM) which stems from the TM2 model developed by **/Heimann, 1996/**. The model solves the continuity equation for a tracer in flux:

$$\frac{\partial}{\partial t}\rho_{air} y + \nabla \rho_{air} \overrightarrow{\mathbf{v}_y} = \mathbf{Q}, \qquad \textbf{Eq. 1}$$

where *y* [$kg_{tracer}\ kg_{air}^{-1}$] is the tracer mixing ratio, ρ_{air} [$kg_{air}\ m^{-3}$] is the air density, $\overrightarrow{\mathbf{v}_y}$ [$m\ s^{-1}$] is the wind vector, and **Q** [$kg_{tracer}\ m^{-3}\ s^{-1}$] represents the volumetric tracer's sources and sinks, for an arbitrary number of tracers on an Eulerian grid **/Heimann and Körner, 2003/**. Three-dimensional tracer advection resolved on the model grid is calculated using the slopes scheme **/Russel and Lerner, 1981/**. Sub-grid scale transport is parameterized: vertical transport due to convective clouds is computed using a simplified version of the cloud mass flux scheme of **/Tiedke, 1989/** and turbulent vertical transport is calculated by stability dependent vertical diffusion according to the scheme of **/Louis, 1979/**. Additionally, horizontal mixing due to mesoscale convection **/Prather et al., 1987/** has been reinstated into the model to improve the representation of interhemispheric exchange **/Monteil et al., 2013/**.

3.3.2.2. Driving meteorology

In this study, the TM3 model will be driven by hourly gridded meteorological re-analysis fields from the Fifth Generation European Centre for Medium Range Weather Forecast (ECMWF) reanalysis ERA-5 **/C3S, 2017/**. These data, which include geopotential height, longitudinal and meridional wind speeds, surface pressure, air temperature and specific humidity, were transformed into advective air mass fluxes and parameterized sub-grid scale convective transport in a pre-processing step and stored in memory **/Heimann and Körner, 2013/**. This approach allows the TM3 model to be run many times with the same pre-processed driving data, without the need for computationally expensive calculation of the dynamic transport equations in every model run.

3.3.2.3. Inversion algorithm

The 4D-VAR variational inversion algorithm of the Jena Carboscope is described in detail in **/Rödenbeck, 2005/**. Here we provide a brief summary. The primary input for flux estimations is a vector the observed tracer mole fractions $\boldsymbol{y_{obs}}$ that contains the total set of measurements at all times and locations. The modelled mole fractions $\boldsymbol{y_{mod}}$ results from the transport a discretized flux field **f**(x,y,t), which varies in time and space. This is formally expressed as:

$$\boldsymbol{y}_{mod} = \boldsymbol{A}\mathbf{f} + \boldsymbol{y}_{ini}, \qquad \textbf{Eq. 2}$$

where $\boldsymbol{y}_{ini}$ is the initial conditions and $\boldsymbol{A}$ is the transport matrix. The inversion seeks to estimate the fluxes **f** that lead to minimum data-model mismatch $(\boldsymbol{y_{obs}} - \boldsymbol{y_{mod}})$ through the minimization of a cost function:

$$J = \frac{1}{2}(\boldsymbol{y_{obs}} - \boldsymbol{y_{mod}})^{\boldsymbol{T}}\boldsymbol{Q_m}(\boldsymbol{y_{obs}} - \boldsymbol{y_{mod}}), \qquad \textbf{Eq. 3}$$

where the diagonal matrix $\boldsymbol{Q_m}$ weights the mole fraction values given their assumed measurement error, location-dependent modelling error and a data-density weighting **/Rödenbeck, 2005/**. The Jena Carboscope typically estimates daily at gridcell scale resolution. Therefore, the problem is ill-posed, because the number of unknowns is larger than the number of measurements. The problem can be regularized by adding *a priori* information.

To simplify the structuring of the *a priori* information such that it reflects process understanding, all the a priori information for each element of the flux vector **f** is supplied in the form of a statistical linear flux model:

$$\mathbf{f} = \mathbf{f}_{fix} + \mathbf{F}\mathbf{p}. \qquad \textbf{Eq. 4}$$

The statistical linear model represents the *a priori* probability distribution of flux vector **f**. The flux vector **f** represents net flux per gridcell per time step. It is composed of a fixed term $\mathbf{f}_{fix}$, which is the *a priori* expectation value $\langle \mathbf{f}_{pri} \rangle$, and an adjustable term, $\mathbf{Fp}$, which determines the deviations around $\langle \mathbf{f}_{pri} \rangle$ (Gaussian distributed). The adjustable term is composed of matrix **F** and vector **p**. Vector **p** is a set of adjustable parameters assumed to be independent, with an a priori expectation value $\langle \mathbf{p}_{pri} \rangle = 0$ and a priori unit variance $\langle \mathbf{p}_{pri}\, \mathbf{p}_{pri}^{\mathbf{T}} \rangle = \frac{\mu}{2}\mathbf{I}$. Each of the elements of vector **p** acts as a multiplier to each one of the columns of the matrix **F**.

The factor μ determines the ratio between a-priori and data constraints. In the limit μ → 0, the a-priori term would vanish, and the a priori covariance given by Eqn. (6) (see below) would go to infinity. This is seen by noting that the cost function J as a whole could be scaled by another arbitrary factor. This should not change the a-posteriori fluxes but only the a-posteriori covariances. In this sense, μ may be considered as a prototype for the many settings that have to be chosen when devising an inversion in a particular application, in particular as a prototype for settings in F. The parameter μ has been highlighted here because (i) it is one of the

most influential settings, (ii) it is directly linked to certain formal mathematical criteria of the Bayesian framework and (iii) when solving the cost function minimization iteratively, there is a particularly easy way to vary μ for the purpose of sensitivity testing. The a-priori scaling parameter μ is generally given as 1 in the standard case. Since the conjugate gradient algorithm used in the optimization can potentially produce negative emissions through overfitting, we scale the parameter μ to ensure that the posterior emissions remain realistic.

The matrix **F** comprises all the *a priori* information about flux uncertainties and correlations. Each column of matrix **F** represents an elementary spatiotemporal flux pattern or base function that is a building block of the total flux uncertainty **/Rödenbeck et al., 2003/**. The extension in space and time of these elementary flux patterns determines the coherent behaviour or correlations of the flux elements.

The matrix **F** is defined as

$$\mathbf{F} = \mathrm{f}_{sh}(x, y, t) \cdot \mathrm{g}_m^{time}(t) \cdot \mathrm{g}_m^{space}(x, y), \qquad \textbf{Eq. 5}$$

where g_m^{time} and g_m^{space} are functions (range from zero to one) determining the temporal and spatial decomposition into statistically independent elements and $\mathrm{f}_{sh}(x, y, t)$ is a discrete spatiotemporal shape function, which determines the local/instantaneous *a priori* standard deviation of the flux **f /Rödenbeck, 2005/**. Since the inversion algorithm will preferably project signals in the data into space and time locations with large *a priori* uncertainty, the shape function provides a spatiotemporal weighting of the flux adjustment and restricts the flux adjustments to prescribed source regions, e.g. land or ocean, or source periods, e.g. the growing season. The *a priori* covariance matrix is

$$\mathbf{Q}_F = \mathbf{F}\mathbf{F}^{\mathbf{T}}. \qquad \textbf{Eq. 6}$$

Furthermore, the Jena Carboscope allows for the representation of the flux vector **f** as the sum of N_{comp} flux components, each of which is represented by its own independent statistical linear flux model:

$$\mathbf{f} = \sum_{i=1}^{N_{comp}} \mathbf{f}_{fix,i} + \mathbf{F}_i\mathbf{p}_i. \qquad \textbf{Eq. 7}$$

Each flux component *i* may correspond to a physical source process, e.g. wetlands, fossil fuel production, or agricultural emissions. Additionally, flux components may correspond to a particular process split into different temporal scales, e.g. mean seasonal cycle, interannual or short-term variability, or spatial scales. Since each component is independent, each component is assigned different *a priori* error covariance structure. Ideally, this approach would allow for the partitioning of the deviations from the *a priori* flux estimate for each flux component considered. This is the case for flux components that are geographically separate, e.g. land vs. ocean fluxes, or temporally separate, e.g. opposite seasonality of wetland emissions and biomass burning in the Tropics. However, due to the nature of CH_4 source and sink processes, there is considerable overlap among the processes contributing to the total flux in each gridcell even with good *a priori* knowledge of their spatiotemporal distribution. When flux components overlap within a data-model mismatch gradient, the deviations from the *a priori* flux estimate calculated by the inversion are attributed to the flux components proportionally to their relative contribution to the overall uncertainty $\mathbf{F}_i/\mathbf{F}$ and to the ratio between the *a priori* flux uncertainty and the data uncertainty.

With this information, the inversion seeks to minimize the cost function that combines the observational and the *a priori* constraint:

$$J = \frac{1}{2}(\mathbf{y}_{obs} - \mathbf{y}_{mod})^{\mathbf{T}}\mathbf{Q}_m(\mathbf{y}_{obs} - \mathbf{y}_{mod}) + \frac{\mu}{2}\mathbf{p}^{\mathbf{T}}\mathbf{p} + C, \qquad \textbf{Eq. 8}$$

where C is a constant that summarizes all parameter independent terms and μ is a tunable parameter that scales the impact of the *a priori* constraint on the Bayesian inversion with respect to atmospheric data constraint. The minimization of the cost

function is done iteratively with respect to the parameters **p** using a Conjugate Gradient algorithm with re-orthogonalization **/Press et al., 2007/**.

3.3.2.4. Atmospheric observations

An initial step in this study shall be the accumulation, intercalibration, and organization of available atmospheric CH_4 dry air mole fraction data. These may include high precision measurements from air samples (flask or canisters taken discretely or at weekly to bi-weekly intervals), in-situ measurements from continuous analyzers averaged at hourly or half-hourly time steps, discrete observations on moving platforms and both ground-based and satellite-based total column measurements.

The Jena Carboscope uses individual mole fraction measurements, picking the corresponding gridbox(es) and interpolating in time between adjacent model time steps to the time of the observation. The individual measurements are used directly, without any previous curve-fitting, smoothing or gap-filling. To avoid data points that the model is unlikely able to represent sufficiently, the measurements are first selected according the recommendations of the data providers relative to the accompanying quality flags.

3.3.2.5. Data uncertainty

Looking back at the cost function (Eq. 8) the diagonal elements of the data covariance matrix, $\mathbf{Q}_m$, which act as a weighting among the data values, represent the sum in quadrature of measurement and modeling uncertainty, or error, for each observation. Measurement errors, σ_{meas}, may be due to natural variations in the measurement equipment (white noise), as well as to equipment precision, repeatability and calibration. Most datasets included an estimate of the measurement error for each individual flask or hourly average. If no estimate of the measurement error was provided, we shall assume 2 ppb for flask and in situ continuous surface measurements **/Dlugokencky et al., 2011/**.

The modeling error, σ_{mod}, reflects the ability of the model to reproduce the observed measurement at a certain location given a correct set of fluxes. The modeling error may be derived from errors in the discretization, parameterization, model structure or driving variables. We shall assume that the modeling error for each gridbox can be represented by the standard deviation of the average monthly CH_4 mole fractions across the adjacent gridboxes (horizontally and vertically including the vertices). For this, we shall generate four dimensional tracer fields using the *a priori* fluxes, averaged them into a twelve month climatology, calculated the standard deviations for each gridbox and stored them on disk. During the *a priori* run of the transport model, the stored model errors shall be loaded, sampled for the corresponding gridbox and month and added in quadrature to the measurement. In the case of total column measurements, the vertical column of standard deviations shall be aggregated to the

retrieval resolution, then added in quadrature weighted by the averaging kernels and then added in quadrature to the measurement uncertainty.

In order to combine stations making hourly measurements with sites where flask samples are taken every two weeks, the Jena Carboscope scales the measurement and the model error by $\sqrt{N^*}$, where *N** is the number of data points for a particular species from a specific station or sampling platform within a temporal correlation period of seven days before and after each measurement. For total column measurements, no data density weighting was applied because the weight of the measurements is strongly diluted in the column.

3.3.2.6. Total-column operator

The use column average mixing ratio data in a Bayesian inverse modeling framework requires the implementation of a column operator because the modeled column average mixing ratios cannot be represented directly as a multiplication of fluxes with the transport matrix (Eq. 1). The implementation of the total column operator and its adjoint within the TM3 model is described in detail in **/Reum, 2012/**.

In short, the four-dimensional discrete mixing ratio fields are sampled at their corresponding TM3 gridcell and time step at each model level *l* creating a vertical profile $\mathbf{y}^{mod}$. Next, the vertical profile must be transformed from the model grid to the retrieval grid. In the original implementation of the column operator, the modeled vertical profile was linearly interpolated or extrapolated to the retrieval grid. Nevertheless, if the mixing ratio profile is not smooth, linear interpolation may cause significant biases [F. Reum, personal communication]. Therefore, the total column operator has been modified to transform the modeled vertical profile to the retrieval grid by making a weighted average, where the weights are the relative pressure thickness of the model levels with respect to the pressure thickness of the retrieval level. This is equivalent to aggregating the tracer and dry air mass to the retrieval grid. Moreover, due to the coarse resolution of the model or to variability between different surface pressure estimates, the surface pressure of the model and the retrieval may not match. If the surface pressure of the retrieval is greater than the surface pressure of the model, the surface pressure of the model is given the value of the surface pressure of the retrieval. This is equivalent to assuming a well-mixed planetary boundary layer such that the mixing ratio is constant in the lowermost model level. On the contrary, if the surface pressure of the retrieval is lower than the surface pressure of the model, only a partial column, starting at the surface pressure of the retrieval, is considered. Once aggregated to the retrieval grid, the average column mixing ratios were calculated according to:

$$\bar{\mathbf{y}}^{\boldsymbol{mod}} = \frac{1}{p_{surf}} \sum_{l=0}^{nlev} \Delta p_l \left[AK_l \cdot y_l^{mod} + (1 - AK_l) \cdot y_l^{prior} \right], \qquad \textbf{Eq. 9}$$

where $\bar{\mathbf{y}}^{mod}$ is the total column average mixing ratio, p_{surf} is the surface pressure, *nlev* is the number of retrieval levels, Δp_l is the pressure level thickness, AK_l is the

averaging kernel's value in the retrieval level *l*, and y_l^{mod} and y_l^{prior} are the modeled and *a priori* mixing ratios at level *l*. The measurement uncertainty as estimated by the retrieval algorithms by propagation of the instrumental and *a priori* errors is provided with the data.

While systematic errors (biases) in the total-column products will be analyzed and dealt with within other WPs in this project, systematic errors still occur in the modeled total column mixing ratios. These systematic errors may be caused by transport errors, errors in the concentration distribution of the photochemical sinks, representation errors due to the different vertical resolutions of the model and the retrieval profiles, or errors in the provided averaging kernels. Particularly, like most off-line transport models, the troposphere-stratosphere exchange in the TM3 model is too fast, leading to a positive bias in the stratosphere and a negative bias in the troposphere.

A common approach has been to define a set of empirical functions describing the spatiotemporal dependence of these systematic errors based on previously optimized tracer fields using direct measurements only **/Houweling et al., 2014/**. These empirical functions will be derived from variables the model run itself and which can be thought of as independent on the surface fluxes.

3.3.2.7. Chemistry implementation

Photochemical destruction of CH_4 and CH_3CCl_3 were represented using the hourly, daily or monthly mean three-dimensional distributions of OH, $O(^1D)$ and Cl extracted from climate-chemistry models or chemistry transport models or diagnostic models. OH, $O(^1D)$ and Cl number densities are prescribed, which means they were not optimized by inverse modeling. Therefore, it is implicitly assumed that their spatiotemporal distributions and magnitudes are realistic. The values were assumed to represent the mean concentration in the middle of the period (e.g. for monthly mean fields, the 16th at 00:00 UTC). Then the OH, $O(^1D)$ and Cl number densities are linearly interpolated in each gridbox for time steps in between.

For CH_4 or CH_3CCl_3, the reaction rate constants with OH, $O(^1D)$ and Cl are well represented in the 200 to 300 K temperature range by the Arrhenius equation:

$$k = A \cdot \exp\left(-\frac{E_A}{R \cdot T}\right), \qquad \textbf{Eq. 10}$$

where *k* is the reaction rate constant [cm^3 $molecules^{-1}$ s^{-1}], *A* [cm^3 $molecules^{-1}$ s^{-1}] is the Arrhenius factor, E_A [J mol^{-1}] is the activation energy, *R* [J mol^{-1} K^{-1}] is the gas constant and *T* [K] is air temperature **/Sander et al., 2006/**. The parameters for Eq. 10 used in this study are summarized in **Table 2**. Temperature is provided by the meteorology driving the model. Empirically determined uncertainty estimates in the reaction rate constants as a function of temperature are not considered in this study. Nevertheless, it must be pointed out that the uncertainty increases as temperature departs from room temperature (~298 K) because fewer measurements are available and because of experimental difficulties.

Table 2: Rate constants for second order reactions represented by Eq. 10 with parameter values from **/Burkholder et al., 2015/**.

Reaction		*A* [cm^3 molecules^{-1} s^{-1}]	E_A/R [K]
CH_4			
	$CH_4 + OH$	2.45×10^{-12}	1775
	$CH_4 + Cl$	7.10×10^{-12}	1270
	$CH_4 + O(^1D)$	1.75×10^{-10}	0
CH_3CCl_3			
	$CH_3CCl_3 + OH$	1.64×10^{-12}	1520
	$CH_3CCl_3 + Cl$	3.0×10^{-12}	1730
	$CH_3CCl_3 + O(^1D)$	3.25×10^{-10}	0

The reaction rate constants are calculated online at each transport model time step. The reaction rate λ [s^{-1}] is then the product of the reaction rate constant *k* and the number density [molecules cm^{-3}] of the oxidizing molecules OH, O(^{1}D) and Cl. The reaction rates were calculated in each gridbox from the surface to the top of the atmosphere. The total amount of tracer *n* destroyed is proportional to the tracer mass itself and to the reaction rate λ.

$$\frac{dn}{dt} = -\lambda \cdot n, \qquad \textbf{Eq. 11}$$

In continuous time, the solution to Eq. 11 is the expression of exponential decay

$$n(t + \Delta t) = n(t) \cdot e^{-\lambda t}, \qquad \textbf{Eq. 12}$$

In our case, λ is the sum of the reaction rates of OH, O(^{1}D) and Cl with tracer *n*. In discrete time, Eq. 12 is integrated with an Eulerian explicit scheme for the tracer mass *n* and the *x*, *y* and *z* slopes.

$$\begin{aligned} n_{i,j,l}^{k+1} &= n_{i,j,l}^{k} \cdot (1 - \lambda \Delta t) \\ nx_{i,j,l}^{k+1} &= nx_{i,j,l}^{k} \cdot (1 - \lambda \Delta t) \\ ny_{i,j,l}^{k+1} &= ny_{i,j,l}^{k} \cdot (1 - \lambda \Delta t) \\ nz_{i,j,l}^{k+1} &= nz_{i,j,l}^{k} \cdot (1 - \lambda \Delta t), \end{aligned} \qquad \textbf{Eq. 13}$$

The explicit scheme has the draw back that instabilities or negative concentrations might occur if the sum of the reaction rates is too large. In this study, instead of adding together the reaction rates of CH_4 with OH, O(^{1}D) and Cl, the reactions were applied sequentially to the tracer mass at the beginning of the model time step, due to the model structure and the ability to quantify the reactions independently.

3.3.2.8. Surface uptake

In contrast to previous atmospheric inverse modeling studies of CH_4, the surface uptake of atmospheric CH_4 was not part of the net surface fluxes. Instead, it was implemented as a zeroth order reaction with prescribed reaction rates occurring only in the surface-most model layer. Formally, this is incorrect because decay rate (modeled by Eq. 13) is applied not only to the tracer mass *n* but also to the slopes n_x, n_y and n_z while, in the TM3 model, surface fluxes within a gridbox are assumed to be homogenous, such that the horizontal slopes n_x and n_y do not change, but the vertical slope n_z is updated as $n_z^{k+1} = n_z^k - Q\Delta t$ approximating a vertical emission density which is delta distributed on the surface. However, this issue is neglected in this setup.

This implementation is mainly useful to represent microbial oxidation of atmospheric methane in the soil. For example, the soil uptake flux calculated by the ***/Curry, 2007/*** model is given by the equation

$$J_0 = g_0 \cdot C_0 \cdot r_c \cdot r_w \cdot \sqrt{D_{soil} k}\ , \qquad \textbf{Eq. 14}$$

where J_0 [mg m^{-2} d^{-1}] is the surface flux, g_0 transforms ppm CH_4 into mg CH_4 m^{-2} d^{-1} based on the ideal gas law, C_0 [ppm] is the atmospheric CH_4 dry air mole fraction, r_c is the fraction of cultivated land, r_w is the fraction of inundated land, D_{soil} [cm^2 s^{-1}] is soil diffusion coefficient and k [s^{-1}] is the first order oxidation rate. After aggregation of the flux estimate onto the TM3, the value of the flux J_0 per gridcell is divided by the value of C_0 used in the model. The mole fraction that substitutes the original value of C_0 was calculated per gridcell per time step during the model run.

3.3.2.9. Initial conditions

Accurate inverse modeling estimates of CH_4 require accurate three-dimensional mixing ratio fields as initial conditions. However, in contrast to other inversion systems, the Jena Carboscope does not explicitly optimize the initial mixing ratios. Instead, the inversion system is able to produce a pulse flux at the first time step of the transport model run which minimizes the mismatch with observations. Nevertheless, this approach may produce unrealistic three-dimensional distributions, which can be accentuated by the oxidation reactions. Therefore, to minimize this effect, it was required to define realistic three-dimensional distributions of the tracers in the atmosphere during first step the forward model run. For this study, we shall use the CAMS CH_4 surface flux inversion to provide the initial conditions.

3.3.2.10. Setup for this study

We will provide optimized emissions spanning from the period over which retrievals are provided. Spin-up and spin-down period of one year and six months respectively shall be added. It is a goal of this study to compare the optimized emissions produced by TM5-4DVAR and the Jena Carboscope. For this we need common data sets for *a priori* emissions, stations and satellite products (GOSAT and TROPOMI). In general we shall approach the CAMS methodology to be able to compare the inversion to CAMS and TM5-4DVAR.

4. Validation data sets

In this section an overview about the data sets used for the validation of the satellite methane data products is presented.

4.1. TCCON

In 2004 the TCCON network was founded in preparation for the validation of the OCO mission, the first dedicated CO_2 satellite mission to be launched. Since then the network has become the standard for validating satellite based column measurements of CO_2 and CH_4. TCCON is a network of inter-calibrated ground-based Fourier transform spectrometers that measure the absorption in the NIR/SWIR of direct sunlight by trace gas species such as CO_2, CH_4, CO, HDO, etc. These measurements are thus much less influenced by atmospheric scattering by cirrus and aerosols than satellite observations of backscattered/reflected sunlight.

For S5P, the TCCON network will be the prime source of validation data. TCCON XCH_4 measurements have been calibrated and validated against the WMO-standard of in-situ measurements using dedicated aircraft campaigns of XCH_4 profiles and their resulting accuracy have been estimated to 0.4% (**/Wunch et al., 2010/**). A complete list of TCCON sites can be found in the TCCON wiki (https://tccon-wiki.caltech.edu/Sites). Most of these stations are used in the routine validation of the TROPOMI XCH4 product to assure that the precision and the bias stay within the mission requirements **/READMe file/**, **/Hasekamp et al, 2019/**.

An important limitation of the TCCON network for validation of satellite retrievals of greenhouse gas concentrations is the limited albedo range that is covered by the TCCON stations. Therefore, product intercomparison at areas which are not covered by the TCCON network is an important supplementary verification of the product, as discussed in **Sect 6.3**. **Table 3** gives an overview of the TCCON stations that are related to the specific target regions specified in **Sect 6.3**.

Table 3: Overview of the stations from the TCCON network selected for validation (500 km radius).

Station	Latitude [degree]	Longitude [degree]	Height [m]
East Trout Lake	54.36	-104.99	500
Park Falls	45.94	-90.27	440
Lamont	36.6	-97.49	320
Darwin	-12.46	130.93	30
Wollongong	-34.41	150.88	30
Ascension Island	7.93	14.41	30

4.2. AirCore

The AirCore is an atmospheric sampler flying under a meteorological balloon. It allows the measurement of the vertical profiles (from the surface up to 30 km of altitude) of atmospheric concentration of greenhouse gases (CO_2, CH_4 and CO). Its concept, initially proposed by NOAA, is extremely simple: it consists of a long tube of stainless steel placed under a meteorological balloon which, in the ascending phase, empties its air by its open end, to fill with air during its downward phase. The captured air column is then interpreted in terms of the vertical gas concentration profile using a Picarro type laser diode analyzer. This system makes it possible to access altitudes not attainable by aircraft flights and to obtain very good vertical resolution.

The main scientific objectives of the AirCore are: 1) Understanding of carbon exchanges along the atmospheric column; 2) Cal/val activities for greenhouse gas space missions; 3) Evaluation of atmospheric chemistry and transport models.

Since 2013, several versions of AirCore have been developped by LMD-CNRS. As part of the French AirCore program (https://aircore.aeris-data.fr/), AirCore-light are launched regularly under meteorological ballons at four sites located in France: Aire-sur-l'Adour, Trainou, Reims and Puy-de-Dôme. These AirCores are deployed in partnership with CNES (the French Space Agency), LSCE (CNRS / CEA / University of Versailles-Saint-Quentin-en -Yvelines), GSMA (CNRS / Université de Reims) and OPGC (CNRS, Blaise Pascal University), in various places around the globe. The development and deployment of AirCores were carried out in the framework of projects funded by the CNRS, CNES, CEA, Ecole polytechnique, IPSL, the European Union and the University from Reims Champagne-Ardenne.

In June 2019, the MAGIC campaign (https://magic.aeris-data.fr/), supported by CNES, CNRS, EUMETSAT and ESA took place in France. As part of IASI/Metop-C validation supported by EUMETSAT and TROPOMI/S5P validation activities, supported by ESA, specific AirCores were launched at the overpass time of Metop-A/B/C and S5P.

For this project, available AirCore profiles from the French AirCore program for the years of interest (mid-2018 – mid-2020) and from the MAGIC2019 campaign will be delivered to the team.

4.3. Aircraft

The Atmospheric Tomography Mission (ATom) comprises dedicated flights of the NASA DC-8 aircraft, designed to provide continuous sampling of tropospheric profiles of trace-gases (including methane) over a wide range of latitudes, sampling each of the 4 seasons in 4 separate campaigns. Each campaign comprises several flights, taking place over several weeks; taken together the measurements in a single campaign typically form a near complete transect of observations spanning North America down to the Southern Pacific (and back).

The final campaign, Atom 4, took place between March and May 2018, providing measurements which can be use in this study to assess retrievals from S5P as well as IASI and CrIS. Atom data should enable the vertical profile information obtained from the TIR and joint SWIR/TIR retrievals to be quantitatively assessed.

Main page for the ATom project: https://espo.nasa.gov/atom/content/ATom

Data access: https://daac.ornl.gov/cgi-bin/dsviewer.pl?ds_id=1581

5. Ongoing activities and projects of relevance

5.1. GHG-CCI+

The ESA GHG-CCI+ project (http://cci.esa.int/ghg) is highly relevant and closely connected to this METHANE+ project in terms of satellite data product and team members.

The focus of GHG-CCI+ is retrieval algorithm development. GHG-CCI+ is carrying out the R&D needed to generate new Greenhouse Gas (GHG) Essential Climate Variable (ECV) satellite-derived CO_2 and CH_4 data products.

These products are column-averaged dry-air mole fractions of carbon dioxide (CO_2), denoted XCO_2, and methane (CH_4), denoted XCH_4, from these satellites / satellite sensors using European scientific retrieval algorithms:

- XCO_2 from OCO-2 and TANSAT,
- XCO_2 and XCH_4 from GOSAT-2 and
- XCH_4 from S5P

in order to allow delivery of GHG ECV data products in-line with GCOS (Global Climate Observing System) requirements **/GCOS-154/ /GCOS-195/ /GCOS-200/**.

GCOS defines the ECV GHG as follows: “Retrievals of greenhouse gases, such as CO2 and CH4, of sufficient quality to estimate regional sources and sinks”.
Once the products are of sufficient quality for a climate service and cover a long enough time period, it is expected that the data will become part of the Copernicus Climate Change Service (C3S, https://climate.copernicus.eu/).

Within GHG-CCI+ satellite-derived XCO_2 (in ppm) and XCH_4 (in ppb) data products are retrieved from satellite radiance observations in the Short-Wave-Infra-Red (SWIR) spectral region. These instruments are used because their measurements are sensitive also to the lowest atmospheric layer and therefore provide information on the regional sources and sinks of CO_2 and CH_4.

5.2. C3S

The focus of the satellite methane retrieval and data product generation sub-project of C3S (Copernicus Climate Change Service; https://climate.copernicus.eu/) is the operational continuation of the non-operational GHG-CCI pre-cursor project (see previous section of the follow-on project GHG-CCI+).

Within that C3S/GHG sub-project satellite-derived atmospheric carbon dioxide (CO_2) and methane (CH_4) Essential Climate Variable (ECV) data products are been generated and provided to ECMWF for inclusion into the Copernicus Climate Data Store (CDS; https://cds.climate.copernicus.eu/) from which users can access these data products and the corresponding documentation.

The C3S/GHG satellite-derived data products are:

- Column-average dry-air mixing ratios (mole fractions) of CO_2 and CH_4, denoted XCO_2 (in parts per million, ppm) and XCH_4 (in parts per billion, ppb), respectively.
- Mid/upper tropospheric mixing ratios of CO_2 (in ppm) and CH_4 (in ppb).

These data products are generated from the satellite instruments SCIAMACHY/ENVISAT and TANSO-FTS/GOSAT (XCO_2 and XCH_4 products) and AIRS and IASI (mid/upper troposphere products).

All data products are available as Level 2 (individual ground pixels) products in NetCDF format.

The XCO_2 and XCH_4 Level 2 products correspond to individual satellite sensors but are also available as merged multi-sensor products. In addition, also merged Level 3 (i.e., gridded) products in Obs4MIPs format are available for the XCO_2 and XCH_4 products. Details are given in **/Reuter et al., 2019/**.

5.3. TROPOMI NL

As part of the Dutch national TROPOMI project funded by NSO, SRON developed the operational methane retrieval code for TROPOMI **/Hasekamp et al, 2019/**. This algorithm is continuously being further improved as part of the NSO funded TROPOMI project. Data products from the beta version of this operational code will be made available also to this project when applicable.

5.4. GALES

SRON runs the GALES project -funded by the Dutch National science foundation NWO- in which the aim is to localise and quantify localised methane emission sources using TROPOMI data. As an example **/Pandey et al., 2019/** published a study on the gas well blow out that occurred in Ohio and was measured and its emissions quantified using TROPOMI.

5.5. GHGSAT – TROPOMI

SRON has an on-going collaboration with GHGSat Inc. to use TROPOMI methane observations to guide GHGSat observations. The idea here is that enhanced methane signals in TROPOMI data are analysed and then used for the targeting of GHGSat which can only observe one area of 12x12 km^2 per orbit. This thus requires GHGSat to target known or assumed locations of strong CH4 sources.

5.6. PROMCOM

Work to apply the TIR retrieval scheme to CrIS and develop a combined TIR(IASI/CrIS)-SWIR(S5P) methane retrieval scheme, to maximise information on lower tropospheric methane, is currently underway through a two-year ESA Living Planet Fellowship awarded to Dr. Knappett (PROMCOM); the results of which will feed directly into the Methane+ project. The ESA fellowship also involves close collaboration with SRON through use of the TROPOMI S5P L2 methane and CO.

6. Current knowledge and science questions to be addressed

6.1. Current knowledge and outstanding science questions

The working group I contribution to the IPCC fifth assessment report lists contemporary radiative forcing's of long-lived greenhouse gases, including 0.93 W/m^2 for CH_4, which is assigned a high level of confidence **/IPCC, 2013/**. The latter is because the main processes that determine the atmospheric burden of methane have been identified and its increase since preindustrial times has been quantified accurately by measurements in ambient air and ice cores.

However, the global budget of methane remains highly uncertain, in particular the relative importance of the main processes and how they have changed over time **/Saunois et al, 2016/**. This is not so important for assessing the present-day climate forcing, but it is highly relevant to the question of how the methane abundance will change in the future and how to effectively reduce its emissions to achieve the internationally agreed climate targets by the end of the century.

Figure 2 illustrates the difficulty of predicting the trend in global methane. In the 1990s its growth rate declined, causing the observed background mixing ratio of methane to be outside of the wide uncertainty envelopes reported in the first four assessment reports. In 2007 the CH_4 increase resumed, with an average growth of 7.4 ppb/yr since then (https://www.esrl.noaa.gov/gmd/ccgg/trends_ch4/).
This has put the CH_4 increase back on track of a scenario that is in between the AR5 scenarios RCP6 and RCP8.5, with corresponding temperature increases by 2100 between 2.75ºC (RCP6) and 4.5ºC (RCP8.5).

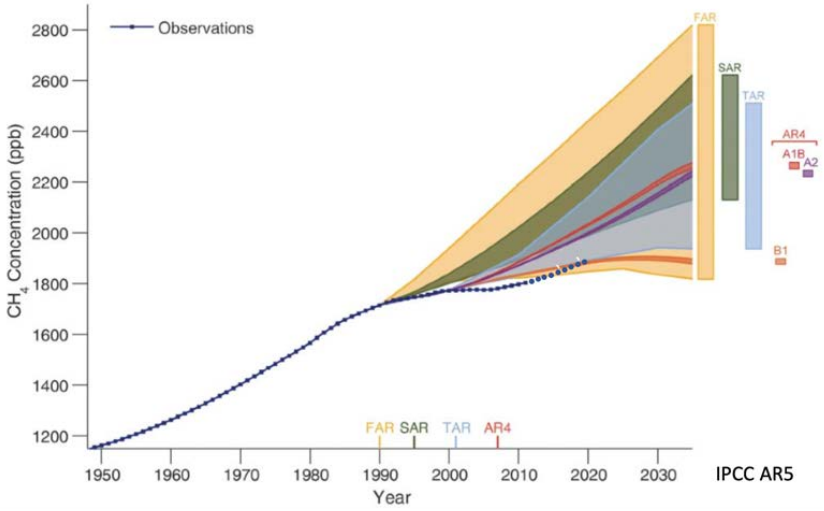

Figure 2: The IPCC projected and observed global atmospheric increase of CH_4.

The reason why the actual CH_4 increase keeps “escaping” the IPCC predictions has been heavily discussed in the scientific literature, without consensus so far. Meanwhile, almost any of the possible scenario’s has been claimed the answer to what happened, ranging from increased emissions from natural wetlands **/Nisbet et al, 2016/**, agriculture **/Schaefer et al, 2016/**, fossil fuel use **/Hausmann et al, 2016/**, up to changes in OH **/Rigby et al, 2017/** or combinations of these factors **/Worden et al, 2017/**.

What makes CH_4 particularly difficult to predict is the large number of contributing processes, with large uncertainties in each of them. The use of atmospheric measurements is complicated by its relatively long lifetime, causing its gradients to be small, with a large contribution of variations in atmospheric transport to the observed variability **/Pandey et al, 2019/**. To distinguish influences from different source categories the use of $\delta^{13}C$ measurements and methane over ethane ratios has arguably been the most successful, although both methods suffer from important limitations also **/Schwietzke et al, 2016; Lan et al, 2019/**.

Compared with carbon dioxide and nitrous oxide, the surface fluxes of methane show a strong spatial variability. This characteristic complicates upscaling methods used in inventories, and also the interpretation of methane measurements from the generally sparse global and regional monitoring networks. However, it does give imaging satellites a potentially important and promising advantage, provided that the resolution and sensitivity of the measurements is high enough. With S5p TROPOMI an important step forward has been made in this direction, although its sensitivity and resolution still limit its application to the largest local sources of methane that exist worldwide.

Since almost all sources of methane are at the Earth surface, the concentration signals are largest inside the planetary boundary layer. The surface sensitivity of total column measurements from TROPOMI could be enhanced further in combination with measurements from thermal IR sounders providing altitude specific information about methane. How to optimal use this information is a scientific question that has not been addressed so far and is a main research priority of this project. Besides the gain in surface sensitivity of a combined SWIR–TIR retrieval product, the vertical profile also contains independent information about methane sources at the surface and its sinks higher up in the atmosphere. This allows us to address the important scientific question of how to separate influences of sources and sinks on the global increase of methane.

6.2. Science cases to be addressed in this study

The main scientific objective of this project is to assess the added value of combining SWIR (TROPOMI) and TIR (IASI, CrIS) measurements of methane. Many new opportunities arise from extending the 2D measurement coverage of TROPOMI into 3D, of which the following have been prioritized and will be further investigated in detail:

1. Improve the attribution and TROPOMI observed local and regional enhancements in total column CH_4

2. Improve the measurement coverage needed to obtain independent information about global sources and sinks of methane

3. Improve the measurement coverage in regions where remote sensing of CH_4 is the most challenging

Ad 1 (attribution of regional signals):

Total column measurements combine information from different altitudes, the origin of which can be different because of wind shear. Height specific in formation helps to disentangle columns enhancements into their directional components, which should improve the capability of the inversion to attribute the observed signal to the correct source region (or the partitioning between multiple source regions). This will be investigated for a region in Asia and South America, where this advantage of combined SWIR-TIR retrievals could be particularly important.

The CH_4 distribution in the atmosphere over South East Asia is strongly influenced by the Indian monsoon circulation. During the summer monsoon air is lifted upwards in the low-pressure system that develops over northern India, in response to the seasonal heating of the Tibetan plateau. As a result, CH_4 rich air masses in the lower troposphere over India, enhanced in part due to fresh inputs from sources over the main land, converge and are lifted upward **/Xiong et al, 2009/**. Aloft, the air diverges in easterly and westerly direction as shown in **Figure 3**. The influence of Chinese CH_4 emissions is clearly separated from that of Indian sources near the surface. In the free troposphere, however, Indian emissions that are transported to China through the monsoon circulation contribute to the total columns CH_4 abundances that are observed by TROPOMI over China. Information on the vertical profile is required to correctly attribute the regional XCH_4 enhancement over China, which we will investigate using combined SWIR-TIR retrievals.

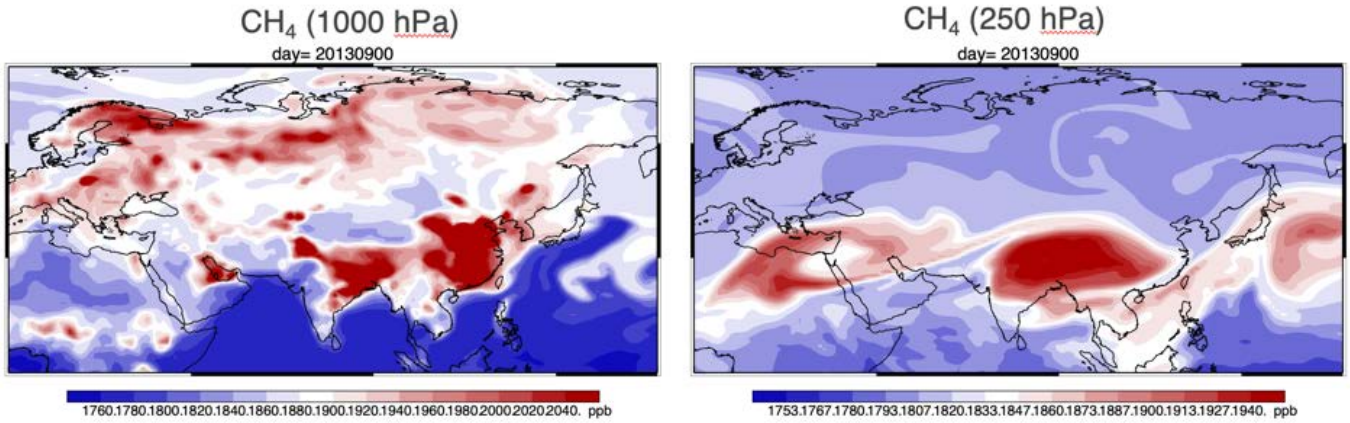

Figure 3: TM5 simulated CH_4 over Asia at 1000 hPa and 250 hPa

The column content of CH_4 over tropical South America is influenced by regional emissions, with tropical wetlands as the most important source in the Amazonian tropical forest. However, the seasonal dynamics in total column CH_4 are dominated by the seasonal movement of the inter tropical convergence zone (ITCZ). The impact of the latitudinally varying position of the ITCZ is large, because it is the transport barrier separating the integrated Northern Hemispheric emissions from the Southern Hemispheric background. It is the dominant mode of large-scale CH_4 variation in the troposphere with a CH_4 gradient across the ITCZ of ~100 ppb. The ITCZ is not a straight vertical barrier, however, causing the latitudinal influence of the Northern Hemisphere to vary with altitude. If a transport model fails to accurately represent this gradient, regional variations in total column CH_4 may be attributed wrongly in an inversion.

To separate CH_4 enhancements due to emissions and the ITCZ movement requires accurate information on the position of the ITCZ and the altitude dependent mixing of Northern Hemispheric air into the Southern hemisphere. The height resolved information provided by the combined use of SWIR and TIR could provide that information. Furthermore, the extended measurement coverage of SWIR-TIR data over the ocean should facilitate the mapping of methane enhancements originating from Amazonian emissions that are transported in westward direction over the Pacific (see **Figure 4**).

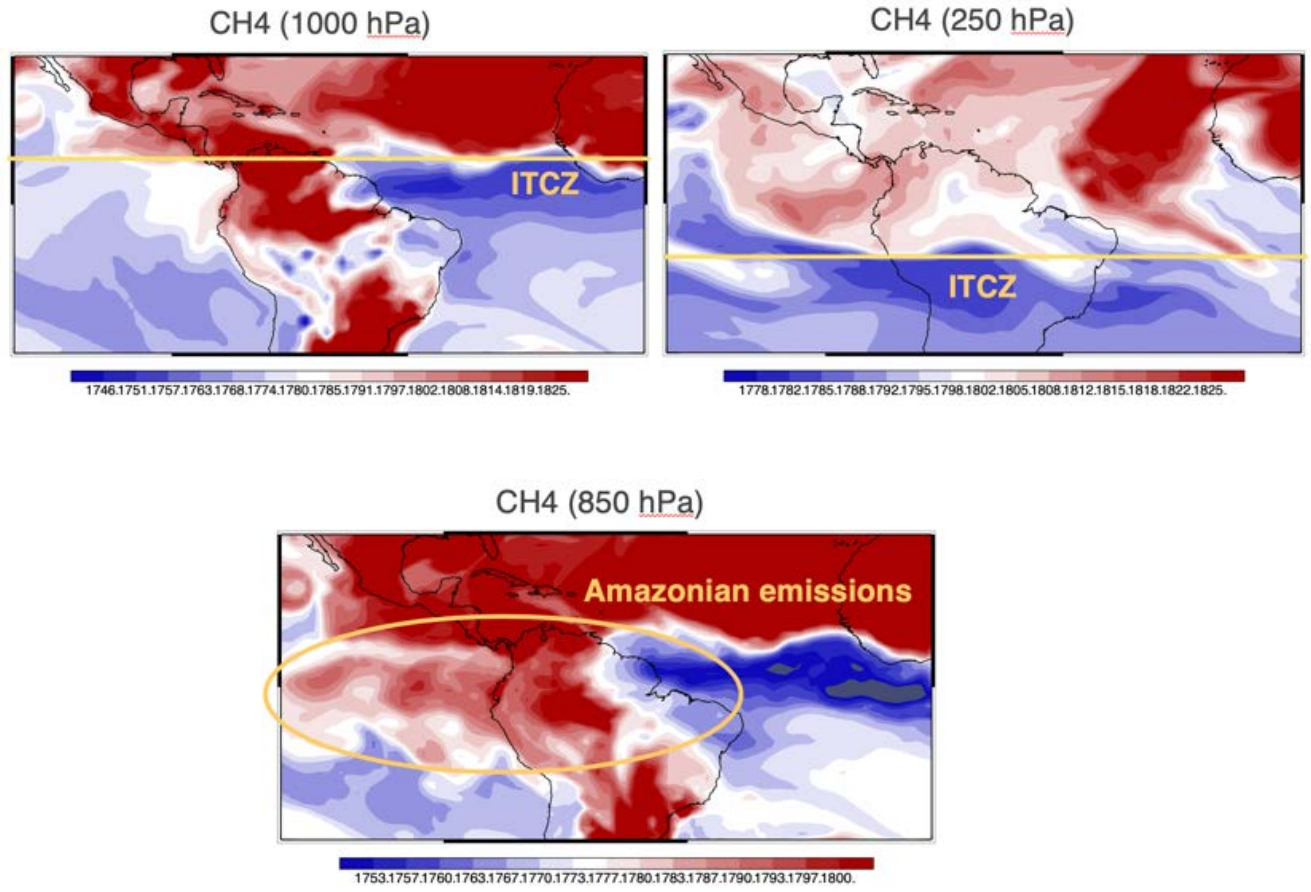

Figure 4: TM5 simulated CH_4 over Amazonia at different pressure levels.

The following activities are planned to investigate the added value of combined SWIR-TIR retrievals for the two cases that are just described.

- Transport model simulations with marked tracers quantifying the contribution of methane emissions from different origins (e.g. India vs China; Amazon vs rest of the world) to the TIR and SWIR retrievals from TROPOMI, IASI, and CrIS that will be generated in the project.
- Comparison of regional CH_4 patterns in TIR and SWIR data to assess the consistency and complementarity of the available datasets, given the corresponding transport model simulations.
- Inverse modelling using either single or combined satellite data products.

Ad 2 (separation between sources and sinks):

The availability of 3D information on the atmospheric methane distribution should facilitate the separation between influence of sources at the surface and sinks in the atmosphere. The longer the transport time between the source and measurement location, the larger the impact of the photochemical sink. For the sink to have a significant impact, however, the transport time has to be significant compared with the lifetime of methane of ~9.5 years.

Figure 5 shows the impact of varying the methane lifetime in TM5. The simulation was setup such that the global budget remained the same by changing the source and sink proportionally, i.e. in a single box model of the atmosphere the changes would cancel out entirely. The largest differences show up in the north-south gradient. Minor changes are found in tropospheric vertical profiles. The experiment did not address the stratosphere, although larger impacts are expected there because of the slow transport times.

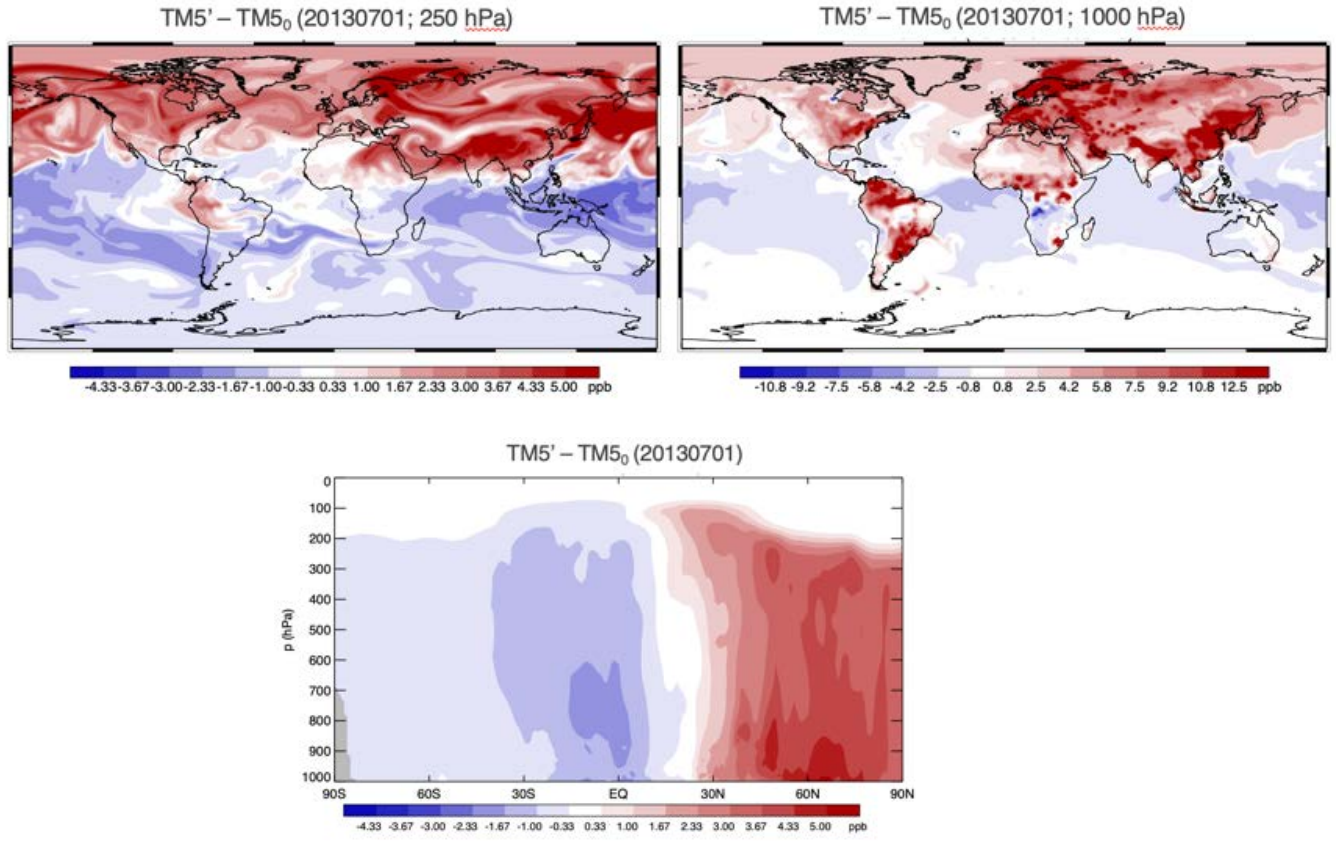

Figure 5: The TM5 simulated sensitivity of global CH_4 mixing ratios to the balance between sources and sinks. $TM5_0$: Standard TM5 setup; TM5': Standard TM5 setup with 10% reduced sources and 10% reduced sinks.

To investigate the added value of combined SWIR-TIR retrievals for separating the sources and sinks of methane, global inversions will be performed in which sources and sinks are optimized. Experiments will be performed using either single or combined satellite data products to assess their impact.

Ad 3 (challenging regions):

Different regions around the Earth may be more or less straightforward to address using satellite remote sensing depending on regionally specific conditions (light availability, poorly constraint conditions such as cloud cover, etc.). A good example of a challenging region that is important for methane emissions in the context of climate change, which is not covered by the cases discussed so far, is the boreal / arctic zone. The impacts of climate change are largest at high latitudes because of arctic amplification, with important implications for methane because of the large reservoir of soil carbon stored in permafrost.

Few attempts have been made to investigate arctic methane emissions using satellite data (e.g. **/Yurganov and Leifer, 2016; Xiong et al, 2010/**). For SWIR measurements this is because of low sun and limitations in the year-around availability of sun light. For TIR measurements the temperature contrast between the surface and the atmosphere is relatively small, and the tropopause is at relatively low altitude with important seasonal dynamics causing methane variations that may be difficult to distinguish from seasonal variations in surface emissions. Furthermore, the surface emissivity is influenced by snow- and ice-covered surfaces.

The extended availability of TROPOMI data due to its large swath and small footprint size improves the coverage of the Arctic zone during summer compared with previous missions. Comparing the available TROPOMI and IASI/CrIS data, using the model to account for difference in their vertical sensitivities, offers a new opportunity to assess the quality and usefulness of the data for studying methane emissions in the boreal and arctic zone.

6.3. Preliminary list of target regions

6.3.1. S5P XCH_4: Challenging regions for retrieval

An initial list of to be studied target regions relevant for this application is given in **Table 4**.

Table 4: Initial list of target regions for: S5P XCH_4: Challenging regions for retrieval.

Target region	Where and when ?	Relevance	Planned investigations	Comments
Canada	Lat:40N-65N Lon:130W-80W May 2018-May 2019	Albedo contrast for low albedo	Comparisons of operational (SRON) and scientific (IUP-UB) XCH_4 with and without bias correction	Time period of one year selected to study seasonal effects
Australia	Lat: 39S-11S Lon: 113E-155E May 2018-May 2019	Albedo contrast for low albedo and albedo-aerosol interaction	-"-	-"-
Sahara	Lat: 5N-35N Lon:20W-40E May 2018-May 2019	High albedo scenes not covered by ground-based stations	-"-	-"-
Atlantic ocean	Orbits with overpass over Ascension Island Lat: 7.93S Lon: 14.41W May 2018-May 2019	Ocean observations with sun-glint geometry	-"-	Time period of one year selected to assure enough cloud-free scenes

6.3.2. S5P XCH_4: Areas with locally elevated XCH_4

Due to the high spatial resolution (7 km) and nearly daily coverage of the TROPOMI/S5P methane retrievals it is possible to detect locally elevated atmospheric methane concentrations originating from localized methane emission sources such as oil, gas and coal fields. An initial list of to be studied target regions relevant for this application is given in **Table 5**.

Table 5: Initial list of target regions for S5P XCH_4 Areas with locally elevated XCH_4.

Target region	Where and when ?	Relevance	Planned investigations	Comments
Turkmenistan, Galkynysh gas field	Latitude: 35±1 °N Longitude: 62±2 °E Initially: 10-Apr-2018	Localized fossil fuel methane emissions (detection, quantification, characteristics)	Comparisons of operational (SRON) and scientific (IUP-UB) XCH_4	See **/Schneising et al., 2019/**
California, Central Valley	Latitude: 36±1.5 °N Longitude: 119±1.5 °W Initially: 20-Feb-2018	-"- In addition: other emissions (cattle, …)	-"-	-"-
Turkmenistan Korpezhe oil/gas field	 Initially: 18-Dec-2017 13-Jan-2019 27-Jan-2019	Localized fossil fuel methane emissions	-"-	See **/Varon et al., 2019/**
Belmont county, Ohio, USA	Latitude: 37° to 41°N Longitude: 79°to 82°W 28-Nov-2017 27-Feb-2018 20-Apr-2018	Methane gas blowout	-"-	See **/Pandey et al., 2019/**

6.3.3. IASI / CrIS CH_4: Challenging regions for retrieval

An initial list of to be studied target regions relevant for this application is given in **Table 6**.

Table 6: Initial list of target regions for IASI XCH_4 Challenging regions for retrieval.

Target region	Where and when ?	Relevance	Planned investigations	Comments
India	Summer 2018 and 2019	Uplift of rice paddies emission by summer monsoon and outflow towards China and the Middle East, mixing local emissions, and long distance transport	Comparisons between RAL and LMD IASI CH_4	
Northwest Brazil		Cloudy region and string CH4 gradient between land and sea	-"-	
High northern latitude		Specific thermodynamic condition, with few knowledge of CH4	-"-	
Saharan Desert	Entire processed period	Difficulty characterising surface emissivity of Saharan sand.	-"-	
North Pacific Ocean (off the west coast of USA and Mexico)	Entire processed period	Possible temperature inversion in area.	-"-	

6.3.4. Science cases to be addressed via regional inverse modelling

The inverse modelling activities will focus primarily on the global scale. However, to investigate the scientific questions and cases that were described in **6.2** the following regions will be studied in further detail.

An initial list of to be studied target regions relevant for this application is given in **Table 7**.

Table 7: Initial list of target regions for Science cases to be addressed via regional inverse modelling.

Target region	Where and when ?	Relevance	Planned investigations	Comments
China / India	70º-120ºE; 10º-35ºN Sept. 2018, 2019	Influence of the Indian summer monsoon on the vertical profile of methane	Tagged tracer simulations; comparison between SWIR and TIR retrievals over south-east China; comparison of inversion optimized emissions from China and India using either SWIR, TIR or Combined SWIR-TIR data	
Amazon basin	45ºW – 100ºW; 15ºS-15ºN NH summer of 2018 and 2019	Influence of the ITCZ dynamics on inversion optimized emissions for the Amazon basin	Tagged tracer simulations; comparison between SWIR and TIR retrievals over tropical South America; comparison of inversion optimized emissions from the Amazon	

			basin using either SWIR, TIR or Combined SWIR-TIR data	
NH Boreal / Arctic	June - August 2018, 2019	Consistency of satellite observed constraints on boreal / arctic CH_4 emissions	Comparison of SWIR and TIR data at high northern latitudes, accounting for differences in vertical sensitivity using the TM5 model.	

7. Consolidated risk analysis and proposed mitigation

The following 'risks' and its mitigation have been taken from the proposal (Sects. 1.2.1 and 1.2.2) and have been updated where appropriate.

Risk-1: use of CrIS data

This project will further develop and implement TIR CH_4 retrievals using CrIS in addition to the IASI-B observations, together with the IMS pre-processor to be applied to MetOp-B and Suomi-NPP[1]. The overall motivation to also look at CrIS is that Suomi-NPP (with CrIS on-board) and S5P (with TROPOMI) are only a few minutes apart and have overlapping swaths. As such it is very interesting to develop a joint (TIR+SWIR) product using those satellites. However, because the RAL TIR scheme developed and well-established for IASI has yet to be adapted to CrIS (in the ESA Living Planet Fellowship) and the IMS scheme has still to be demonstrated extensively for Suomi NPP CrIS & ATMS, we do not yet have a clear assessment of the quality of the CrIS CH_4 data. If the CrIS CH_4 data product is comparable in quality of the IASI-B CH_4 product the project will also deliver a CrIS CH4 product. If the CH_4 data from CrIS is worse than IASI-B we will not generate a large dataset based on CrIS as it makes no sense to generate an inferior TIR CH4 product. The best TIR product (either IASI-B or CrIS) will be used for the generation of the 2 year TIR+SWIR dataset.

Mitigation-1

For the TIR and (TIR+SWIR) CH_4 retrieval product we do not rely solely on CrIS. As a start we use the already well developed IASI-B TIR CH4 product, which also serves as a fallback in case the quality of the CrIS-related products is not as good as the comparable IASI-B product. Note also that current uncertainties surrounding the use of CrIS will be reduced by ongoing work within PROMCOM before the planned start of this project

Risk-2: combined TIR-SWIR retrieval

The basis for the combined TIR-SWIR retrieval scheme is to be developed and demonstrated in the Living Planet Fellowship. We do not yet know the quality of the joint retrievals or the extent to which they may be limited by currently unknown technical issues. E.g. certain kinds of bias between SWIR and TIR may be difficult to accommodate in the joint retrieval. There is therefore some risk (which we will of course seek to minimize) that it becomes clearly not useful (or not feasible due to schedule reasons) to fully analyse joint SWIR/TIR retrievals for this project.

[1] The Infrared and Microwave Sounding (IMS) scheme pre-retrieves atmospheric temperature and humidity profiles, surface temperature and spectral emissivity for use in the TIR methane retrieval.

Mitigation-2

SWIR/TIR retrieval work will also be more advanced by the planned start of this project, through ongoing activities in the PROMCOM fellowship. Joint SWIR/TIR retrievals for at least 1 year of data will be evaluated at an early stage, using the methodology to be applied in this study. Limiting issues will be identified such that they can be addressed through the additional development work in this project. Related points of further work would also be identified in road-map developed in task 4.

Risk-3: results EUMETSAT study not available

There is a risk that the upcoming Eumetsat study on Independent validation of IASI CH4 products, expected to inter-compare and validate RAL and LMD IASI methane products with ground and airborne measurements, may not provide clear results in a timely enough manner to be taken into account within WP2000.

Mitigation-3

We proposed not to start before 1 Jan 2020 to be able to take most benefit from the EUMETSAT study. In fact the project started 22 Jan 2020. However, the EUMETSAT study had some delay in starting (KO September), and further delay with actual work to October. However, while the Eumetsat IASI CH_4 intercomparison study should and could be informative, it is not vital for the work of this project which also builds on the extensive validation activities already performed by the developing teams, which can be extended to recent IASI-B measurements, and the targeted comparison efforts planned for WP2000.

In addition, we will contact EUMETSAT to inquire for early access to intermediate results of the study.

Risk-4: access to recent validation data

Access to validation data for the -very recent- time period studied in this proposal (mid 2018 – mid 2020).

Mitigation-4

SRON has direct contact with a number of TCCON PIs for the validation of the TROPOMI CH_4 product. This helps in getting as quick as possible access to the SWIR validation data.

Prof.dr. Huilin Chen (University of Groningen) is a collaborator to this proposal and as such can provide early access to AirCore data for which he is principal investigator. This includes AirCores at Sodankyla (2018-2019), Trainou (June 2019), Kiruna (September 2020) and possibly (TBC) Paramaribo, Suriname and de Bilt, The Netherlands.

Fast access to AirCore data taken over France is facilitated by having dr. Cyril Crevoisier as part of the project team. Dr. Crevoisier is leading the French AirCore program at 4 French supersites. AirCore CH_4 vertical profiles to be provided here include monthly launches at Aire-sur-l'Adour, regular launches at Trainou and Reims stations, and profiles acquired during the MAGIC2019 campaign which is a French-national campaign funded in part by ESA. During this campaign also CH4 vertical profiles measured with the SAFIRE/Falcon20 will be available.

Risk-5: Inverse modelling challenges

The inverse modelling systems are available, and their application to TROPOMI and IASI (or CrIS) data is relatively straightforward. In TM5-4DVAR, the optimization of methane sinks is implemented in its application to MCF data. However, no split is made between the northern and southern hemisphere like we are proposing here. Since this follows the same logic no specific difficulty is foreseen. Nevertheless, adjoint coding in a large model system is not trivial and could take more time than planned.

The combined use of TIR and SWIR data relies on the model being capable of realistically reproducing the vertical gradient of methane. Earlier studies confirmed that the model is performing sufficiently well in the troposphere. However, latitude dependent deviations have been found in the lower stratosphere **/Monteil et al, 2013/,** pointing to errors in the modelled stratosphere-troposphere exchange or the vertical mixing in the stratosphere. This is a known problem in transport modeling of methane, and has been found in many models **/Patra et al, 2011/**. Cressot et al **/Cressot et al., 2014/** report a consistent integration of IASI and GOSAT data in LMDz despite this problem. Therefore, it may turn out not be to so critical, but will nevertheless need careful attention. The availability of Aircore data in this project will greatly facilitate testing the performance of the model in the UTLS, which is part of what we want to investigate. However, if the model turns out to be the performance limiting factor then this is not an easy problem to solve.

Mitigation-5

The optimization of sinks in TM5-4DVAR will be implemented in steps, starting with the combined use of SWIR and TIR data without sink optimization, followed by optimization using a single scaling factor, followed by sink optimization by hemisphere. This incremental approach will not only provide insight in how the system responds to adding degrees of freedom to the sink side of the problem, it also provides us with useful intermediate results in case progress is slower than foreseen. In the worst case we could complete our assessment using only a global scaling of OH. However, we would be interested to investigate whether the data provide independent constraints on hemispheric sinks, given the ongoing scientific debate on this topic **/Patra et al, 2014/** .

If the combined use of SWIR and TIR data in TM5-4DVAR turns out to be problematic because of transport model errors in the lower stratosphere then we will

implement an ad hoc bias correction to account for this problem, similar to the bias correction that has been used so far when combining GOSAT and surface data. In this case, a simple function of latitude and season was sufficient, limiting the amount of information provided by the data that is not available for optimizing sources and sinks **/Segers and Houweling, 2018/**.

Other:

The amount of data generated by TROPOMI may be a challenge in order to use it in the inversion system. Several strategies are being discussed, for example reading in the data during the model run (less memory usage but longer run times) or using “superobs” which still are a subject of active research.

8. Acronyms and abbrevations

Acronym	Meaning
ACOS	Atmospheric CO2 Observations from Space (algorithm)
ATBD	Algorithm Theoretical Basis Document
ATOM	Atmospheric Tomography Mission
BESD	Bremen optimal estimation DOAS
CAMS	Copernicus Atmosphere Monitoring Service
C3S	Copernicus Climate Change Service
CCI	Climate Change Initiative (of ESA)
CrIS	Cross-track Infrared Sounder
DOAS	Differential Optical Absorption Spectroscopy
EMMA	Ensemble median algorithm
ENVISAT	Environmental Satellite
ESA	European Space Agency
FOCAL	Fast atmospheric trace gas retrieval (algorithm)
FP	Full Physics
GALES	Gas Leaks from Space
GHG	Greenhouse Gas
GHGSat	Greenhouse Gas Satellite
GHG-CCI	Greenhouse Gas project of ESA's Climate Change Initiative (CCI)
GOSAT	Greenhouse Gases Observing Satellite
IASI	Infrared Atmospehric Sounding Interferometer
IUP-UB	Institute of Environmental Physics (Institut für Umweltphysik), University of Bremen, Germany
L1	Level 1
L2	Level 2
LMD	Laboratoire de Meteorologie Dynamique
MPI	Max Planck Institute
NIES	National Institute for Environmental Studies
NIR	Near Infra Red (band)
NRT	Near Real Time
OCO	Orbiting Carbon Observatory
OCO-2	Orbiting Carbon Observatory No. 2
PROMCOM	ESA Living Planet Fellowship awarded to Dr. Knappett, RAL
RAL	Rutherford Appleton Laboratory
RemoTeC	SRON retrieval algorithm
RMS	Root Mean Square
RMSE	Root Mean Square Error
RSS	Root Sum Square
RTM	Radiative Transfer Model

SCIAMACHY	Scanning Imaging Absorption Spectrometers for Atmospheric Chartography
SNR	Signal to Noise Ratio
SRON	SRON Netherlands Institute for Space Research
SUOMI NPP	SUOMI National Polar-orbiting Partnership
SWIR	Short Wave Infrared
SZA	Solar Zenith Angle
TCCON	Total Carbon Column Observing Network
TROPOMI	TROPOsheric Monitoring Instrument
VERIFY	Verifying greenhouse gas emissions (EU H2020 project)
VIIRS	Visible-Infrared Imager and Radiometer Suite

9. URL overview table

URL	Explanation
https://iasi.cnes.fr/en/IASI/index.htm	IASI official website
http://eodg.atm.ox.ac.uk/user/dudhia/iasi/documents/PDF_IASI_LEVEL_1_PROD_GUIDE.pdf	Description of IASI L1 data
https://aircore.aeris-data.fr/	French AirCore program official website
https://magic.aeris-data.fr/	MAGIC campaign official website
https://tcconwiki.caltech.edu/Sites	TCCON wiki
https://aircore.aeris-data.fr/	AirCore program
https://espo.nasa.gov/atom/content/ATom	Main page for the ATom project
https://daac.ornl.gov/cgi-bin/dsviewer.pl?ds_id=1581	Atom data access
http://cci.esa.int/ghg	ESA GHG-CCI+ project
https://climate.copernicus.eu/	C3S website
https://cds.climate.copernicus.eu/	Copernicus Climate Data Store (CDS)
https://verify.lsce.ipsl.fr/	VERIFY website
https://atmosphere.copernicus.eu/	CAMS website
http://www.iup.uni-bremen.de/carbon_ghg/products/tropomi_wfmd/	IUP-Bremen TROPOMI WFMD website
http://www.ceda.ac.uk/	CEDA website
https://www.esrl.noaa.gov/gmd/ccgg/trends_ch4/	NOAA methane trends website
https://s5phub.copernicus.eu/	S5P data hub

10. References

/Alexe et al., 2015/ Alexe, M., P. Bergamaschi, A. Segers, R. Detmers, A. Butz, O. Hasekamp, S. Guerlet, R. Parker, H. Boesch, C. Frankenberg, R. A. Scheepmaker, E. Dlugokencky, C. Sweeney, S. C. Wofsy, E. A. Kort, Inverse modelling of CH4 emissions for 2010-2011 using different satellite retrieval products from GOSAT and SCIAMACHY, Atmos. Chem. Phys., 15, 113--133, doi:10.5194/acp-15-113-2015, 2015.

/Armante et al., 2016/ Armante R., Scott N.A., Crevoisier C., Capelle V., Crépeau L., Jacquinet, N. and Chédin A, Evaluation of spectroscopic databases through radiative transfer simulations compared to observations. Application to the validation of GEISA 2015 with IASI and TCCON, *J. Mol. Spectrosc.*, 327, 180-192, 2016.

/Bergamaschi et al, 2013/ Bergamaschi, P., S. Houweling, A. Segers, M. Krol, C. Frankenberg, R. A. Scheepmaker, E. Dlugokencky, S. C. Wofsy, E. A. Kort, C. Sweeney, T. Schuck, C. Brenninkmeijer, H. Chen, V. Beck, C. Gerbig, Atmospheric CH4 in the first decade of the 21st century: Inverse modeling analysis using SCIAMACHY satellite retrievals and NOAA surface measurements. 2013

/Bousquet et al., 2011/ Bousquet, P., Ringeval, B., Pison, I., Dlugokencky, E. J., Brunke, E.-G., Carouge, C., Chevallier, F., Fortems-Cheiney, A., Frankenberg, C., Hauglustaine, D. A., Krummel, P. B., Langenfelds, R. L., Ramonet, M., Schmidt, M., Steele, L. P., Szopa, S., Yver, C., Viovy, N., and Ciais, P.: Source attribution of the changes in atmospheric methane for 2006–2008, Atmos. Chem. Phys., 11, 3689-3700, https://doi.org/10.5194/acp-11-3689-2011, 2011.

/Buchwitz et al., 2017/ Buchwitz, M., Reuter, M., Schneising, O., Hewson, W., Detmers, R. G., Boesch, H., Hasekamp, O. P., Aben, I., Bovensmann, H., Burrows, J. P., Butz, A., Chevallier, F., Dils, B., Frankenberg, C., Heymann, J., Lichtenberg, G., De Maziere, M., Notholt, J., Parker, R., Warneke, T., Zehner, C., Griffith, D. W. T., Deutscher, N. M., Kuze, A., Suto, H., and Wunch, D.: Global satellite observations of column-averaged carbon dioxide and methane: The GHG-CCI XCO_2 and XCH_4 CRDP3 data set, Remote Sensing of Environment 203, 276-295, http://dx.doi.org/10.1016/j.rse.2016.12.027, 2017.

/Buchwitz et al., 2019/ Buchwitz, M., Reuter, M., Schneising-Weigel, O., Aben, I., Wu, L., Hasekamp, O. P., Boesch, H., Di Noia, A., Crevoisier, C. and Armante, R.: Product Quality Assessment Report (PQAR) – Main document for Greenhouse Gas (GHG: CO_2 & CH_4) data set CDR 3 (2003-2018), Technical Report Copernicus Climate Change Service (C3S), version 3.1, 3-11-2019, pp. 103, access: http://www.iup.uni-bremen.de/carbon_ghg/docs/C3S/CDR3_2003-2018/PQAR/C3S_D312b_Lot2.2.3.2-v1.0_PQAR-GHG_MAIN_v3.1.pdf, 2019.

/Burkholder et al., 2015/ Burkholder, J. B., Sander, S. P., Abbatt, J. P. D., Barker, J. R., Huie, R. E., Kolb, C. E., Kurylo, M. J., Orkin, V. L., Wilmouth, D. M., & Wine, P. H. (2015). *Chemical Kinetics and Photochemical Data for Use in Atmospheric Studies, Evaluation No. 18*. Jet Propulsion Laboratory. http://jpldataeval.jpl.nasa.gov

/Butz et al., 2011/ Butz, A., Guerlet, S., Hasekamp, O., Schepers, D., Galli, A., Aben, I., Frankenberg, C., Hartmann, J.-M., Tran, H., Kuze, A., Keppel-Aleks, G., Toon, G., Wunch, D., Wennberg, P., Deutscher, N., Griffith, D., Macatangay, R., Messerschmidt, J., Notholt, J., and Warneke, T.: Toward accurate CO_2 and CH_4 observations from GOSAT, Geophys. Res. Lett., doi:10.1029/2011GL047888, 2011.

/Butz et al., 2012/ Butz, Galli, Hasekamp, Landgraf, Tol, Aben, TROPOMI aboard Sentinel-5 Precursor : prospective performance of CH4 retrievals for aerosol and cirrus loaded atmospheres, Remote Sensing Environment, doi:10.1016/j.rse.2011.05.030, 2012.

/C3S, 2017/ Copernicus Climate Change Service C3S. (2017). *ERA5: Fifth generation of ECMWF atmospheric reanalyses of the global climate*. https://cds.climate.copernicus.eu/cdsapp#!/home

/Capelle et al., 2018/: Capelle, V., Chédin, A., Pondrom, M., Crevoisier, C., Armante, R., Crépeau, L., and Scott, N.A., Infrared dust aerosol optical depth retrieved daily from IASI and comparison with AERONET over the period 2007–2016, Remote Sens. Env., 206, 15–32, doi:10.1016/j.rse.2017.12.008, 2018.

/Crevoisier et al., 2009a/: Crevoisier, C., Chédin, A., Matsueda, H., et al., First year of upper tropospheric integrated content of CO_2 from IASI hyperspectral infrared observations, *Atmos. Chem. Phys.*, 9, 4797-4810, 2009.

/Crevoisier et al. 2009b/ Crevoisier, C., Nobileau, D., Fiore, A., Armante, R., Chédin, A., and Scott, N. A.: Tropospheric methane in the tropics – first year from IASI hyperspectral infrared observations, Atmos. Chem. Phys., 9, 6337–6350, doi:10.5194/acp-9-6337-2009, 2009b.

/Crevoisier et al., 2013/ Crevoisier, C., Nobileau, D., Armante, R., et al., The 2007–2011 evolution of tropical methane in the mid-troposphere as seen from space by MetOp-A/IASI, *Atmos. Chem. Phys.*, 13, 4279-4289, 2013.

/Curry 2007/ Curry, C. L. (2007). Modeling the soil consumption of atmospheric methane at the global scale. *Global Biogeochemical Cycles*, *21*(4). https://doi.org/10.1029/2006GB002818.

/Detmers & Hasekamp, 2016/ Detmers, R., & Hasekamp, O. (2016). *Product User Guide (PUG) for the RemoTeC XCH4 PROXY GOSAT Data Product v2.3.8*.

/Dlugokencky et al., 2009/ Dlugokencky, E. J., Bruhwiler, L., White, J. W. C., Emmons, L. K., Novelli, P. C., Montzka, S. A., ... Gatti, L. V. (2009). Observational constraints on recent increases in the atmospheric CH 4 burden. *Geophysical Research Letters*, *36*(18), L18803. https://doi.org/10.1029/2009GL039780.

/Dlugokencky et al., 2011/ Dlugokencky, E. J., Nisbet, E. G., Fisher, R., & Lowry, D. (2011). Global atmospheric methane: Budget, changes and dangers. *Philosophical Transactions of the Royal Society A: Mathematical, Physical and Engineering Sciences*, *369*(1943), 2058–2072. https://doi.org/10.1098/rsta.2010.0341

/Dudhia, A/ Dudhia, A., The Reference Forward Model (RFM), J. Quant. Spectrosc. Ra., 186, 243–253, https://doi.org/10.1016/j.jqsrt.2016.06.018, 2016.

/Feng et al., 2017/ Feng, L., Palmer, P. I., Bösch, H., Parker, R. J., Webb, A. J., Correia, C. S. C., Deutscher, N. M., Domingues, L. G., Feist, D. G., Gatti, L. V., Gloor, E., Hase, F., Kivi, R., Liu, Y., Miller, J. B., Morino, I., Sussmann, R., Strong, K., Uchino, O., Wang, J., and Zahn, A.: Consistent regional fluxes of CH4 and CO2 inferred from GOSAT proxy XCH4 : XCO2 retrievals, 2010–2014, Atmos. Chem. Phys., 17, 4781-4797, https://doi.org/10.5194/acp-17-4781-2017, 2017.

/GCOS-154/ Global Climate Observing System (GCOS), SYSTEMATIC OBSERVATION REQUIREMENTS FOR SATELLITE-BASED PRODUCTS FOR CLIMATE, Supplemental details to the satellite-based component of the "Implementation Plan for the Global Observing System for Climate in Support of the UNFCCC (2010 update)", Prepared by World Meteorological Organization (WMO), Intergovernmental Oceanographic Commission, United Nations Environment Programme (UNEP), International Council for Science, Doc.: GCOS 154, link: http://cci.esa.int/sites/default/files/gcos-154.pdf, 2011.

/GCOS-195/ Status of the Global Observing System for Climate. GCOS-195. Link: https://library.wmo.int/pmb_ged/gcos_195_en.pdf, 2015.

/GCOS-200/ The Global Observing System for Climate: Implementation Needs, GCOS 2016 Implementation Plan, World Meteorological Organization (WMO), GCOS-200 (GOOS-214), pp. 325, link: https://library.wmo.int/opac/doc_num.php?explnum_id=3417, 2016.

/Gilbert and Lemaréchal, 1989/ Gilbert, J. C., & Lemaréchal, C. (1989). Some numerical experiments with variable-storage quasi- Newton algorithms. *Mathematical Programming*, *45*(1), 407–435. https://doi.org/10.1007/BF01589113.

/Granier et al., 2011/ Granier, C., Bessagnet, B., Bond, T., D'Angiola, A., van der Gon, H., Frost, G. J., ... van Vuuren, D. P. (2011). Evolution of anthropogenic and biomass burning emissions of air pollutants at global and regional scales during the 1980--2010 period. *Climatic Change*, *109*(1), 163. https://doi.org/10.1007/s10584-011-0154-1.

/Han et al., 2013/ Han, Y. et al. Suomi NPP CrIS measurements, sensor data record algorithm, calibration and validation activities, and record data quality. *J. Geophys. Res.* **118**, 12734–12748 (2013).

/Hasekamp et al., 2019/ Hasekamp, Lorente, Hu, Butz, aan den Brugh, Landgraf, ATBD for S5P Methane retrieval, SRON-S5P-LEV2-RP-001, issue1.10, 2019.

/Heimann 1996/ Heimann, M. (1996). *The Global Atmospheric Tracer Model TM2* (No. 10). Deutsches Klimarechenzentrum. https://www.researchgate.net/publication/228731822_The_Global_Atmospheric_Tracer_Model_TM2

/Heimann and Körner 2003/ Heimann, M., & Kör*ner, S. (2003). The Global Atmospheric Tracer Model TM3 Model Description and User's Manual Release 3.8a (No. 5). Max Planck Institute for Biogeochemistry. http://www.bgc-*

jena.mpg.de/mpg/websiteBiogeochemie/Publikationen/Technical_Reports/tech_report5.pdf

/Heymann et al., 2012/ Heymann, J., H. Bovensmann, M. Buchwitz, J. P. Burrows, N. M. Deutscher, J. Notholt, M. Rettinger, M. Reuter, O. Schneising, R. Sussmann, and T. Warneke SCIAMACHY WFM-DOAS XCO_2: reduction of scattering related errors, Atmos. Meas. Tech., 5, 2375-2390, 2012.

/Heymann et al., 2015/ Heymann, J., Reuter, M., Hilker, M., Buchwitz, M., Schneising, O., Bovensmann, H., Burrows, J. P., Kuze, A., Suto, H., Deutscher, N. M., Dubey, M. K., Griffith, D. W. T., Hase, F., Kawakami, S., Kivi, R., Morino, I., Petri, C., Roehl, C., Schneider, M., Sherlock, V., Sussmann, R., Velazco, V. A., Warneke, T., and Wunch, D.: satellite XCO_2 retrievals from SCIAMACHY and GOSAT using the BESD algorithm, Atmos. Meas. Tech., 8, 2961-2980, 2015.

/HITRAN2016/ Gordon et al., The HITRAN2016 molecular spectroscopic database, J. Quant. Spectrosc. Radiat. Transfer, 203, 3-69, 2017.

/Holtslag and Boville, 1993/ Holtslag, A. A. and Boville, B. A.: Local versus nonlocal boundary layer diffusion in a global climate model, J. Climate, 10, 1825–1842, 1993.

/Houweling et al, 1998/ Houweling, S., Dentener, F., & Lelieveld, J. (1998). The impact of nonmethane hydrocarbon compounds on tropospheric photochemistry. *Journal of Geophysical Research: Atmospheres*, *103*(D9), 10673–10696. https://doi.org/10.1029/97JD03582.

/Houweling et al., 2014/ Houweling, S., Krol, M., Bergamaschi, P., Frankenberg, C., Dlugokencky, E. J., Morino, I., Notholt, J., Sherlock, V., Wunch, D. B., Beck, V., Gerbig, C., Chen, H., Kort, E. A., Röckmann, T., & Aben, I. (2014). A multi-year methane inversion using SCIAMACHY, accounting for systematic errors using TCCON measurements. *Atmospheric Chemistry and Physics*, *14*(8), 3991–4012. https://doi.org/10.5194/acp-14-3991-2014

/Houweling et al., 2017/ Houweling, S., Bergamaschi, P., Chevallier, F., Heimann, M., Kaminski, T., Krol, M., Michalak, A. M., and Patra, P.: Global inverse modeling of CH4 sources and sinks: An overview of methods, Atmos. Chem. Phys., 17, 235-256, doi:10.5194/acp-17-235-2017, 2017.

/Hu et al., 2018/ Hu, Landgraf, Detmers, Borsdorff, aan den Brugh, Aben, Butz and Hasekamp, Geophys.Res.Lett., Towards global mapping of methane with TROPOMI: First results and intercomparison, doi: 10.1002/2018GL077259, 2018.

/Huijnen et al., 2010/ Huijnen, V., Williams, J., van Weele, M., van Noije, T., Krol, M., Dentener, F., ... Pätz, H.-W. (2010). The global chemistry transport model TM5: description and evaluation of the tropospheric chemistry version 3.0. *Geoscientific Model Development*, *3*(2), 445–473. https://doi.org/10.5194/gmd-3-445-2010

/IASI Level 1 Product Guide/ Available from http://eodg.atm.ox.ac.uk/user/dudhia/iasi/documents/PDF_IASI_LEVEL_1_PROD_GUIDE.pdf.

/IPCC, 2013/ IPCC, 2013: Climate Change 2013: The Physical Science Basis. Contribution of Working Group I to the Fifth Assessment Report of the Intergovernmental Panel on Climate Change [Stocker, T.F., D. Qin, G.-K. Plattner, M. Tignor, S.K. Allen, J. Boschung, A. Nauels, Y. Xia, V. Bex and P.M. Midgley (eds.)]. Cambridge University Press, Cambridge, United Kingdom and New York, NY, USA, 1535 pp., 2013

/IPCC, 2018/ IPCC, 2018: Global warming of 1.5°C. An IPCC Special Report on the impacts of global warming of 1.5°C above pre-industrial levels and related global greenhouse gas emission pathways, in the context of strengthening the global response to the threat of climate change, sustainable development, and efforts to eradicate poverty [V. Masson-Delmotte, P. Zhai, H. O. Pörtner, D. Roberts, J. Skea, P.R. Shukla, A. Pirani, W. Moufouma-Okia, C. Péan, R. Pidcock, S. Connors, J. B. R. Matthews, Y. Chen, X. Zhou, M. I. Gomis, E. Lonnoy, T. Maycock, M. Tignor, T. Waterfield (eds.)].

/Jacquinet-Husson et al., 2011/ Jacquinet-Husson, N., Crepeau, L., Armante, R., et al. (2011). The 2009 edition of the GEISA spectroscopic database. J. Quant. Spectrosc. Radiat. Transf. 112, 2395–2445. doi:10.1016/j.jqsrt.2011.06.004.

/Janssens-Maenhout, 2017/ Janssens-Maenhout, G., Crippa, M., Guizzardi, D., Muntean, M., Schaaf, E., Dentener, F., Bergamaschi, P., Pagliari, V., Olivier, J. G. J., Peters, J. A. H. W., van Aardenne, J. A., Monni, S., Doering, U., and Petrescu, A. M. R.: EDGAR v4.3.2 Global Atlas of the three major Greenhouse Gas Emissions for the period 1970–2012, Earth Syst. Sci. Data Discuss., https://doi.org/10.5194/essd-2017-79, 2017.

/Jöckel et al., 2006/ Jöckel, P., Tost, H., Pozzer, A., Brühl, C., Buchholz, J., Ganzeveld, L., ... Lelieveld, J. (2006). The atmospheric chemistry general circulation model ECHAM5/MESSy1: consistent simulation of ozone from the surface to the mesosphere. *Atmospheric Chemistry and Physics*, *6*(12), 5067– 5104. https://doi.org/10.5194/acp-6-5067-2006

/Kaiser et al., 2012/ Kaiser, J. W., Heil, A., Andreae, M. O., Benedetti, A., Chubarova, N., Jones, L., Morcrette, J.-J., Razinger, M., Schultz, M. G., Suttie, M., and van der Werf, G. R.: Biomass burning emissions estimated with a global fire assimilation system based on observed fire radiative power, Biogeosciences, 9, 527–554, doi:10.5194/bg-9-527-2012, 2012.

/Kim et al., 2019/ Kim, E., Lyu, C.-H. J., Anderson, K., Leslie, R. V., and Blackwell, W. J. (2014), S-NPP ATMS instrument prelaunch and on-orbit performance evaluation, *J. Geophys. Res. Atmos.*, 119, 5653– 5670, doi:10.1002/2013JD020483.

/Knappett et al., 2018/ Knappett, D., Siddans, R., Walker, J., and Kerridge, B., Rider to: IASI CH4 Operational Retrieval Feasibility – Optimal Estimation Method, Final Report, Eumetsat Contract, EUM/CO/14/4600001315/RM, 2018.

/Krol et al., 2005/ Krol, M., Houweling, S., Bregman, B., van den Broek, M., Segers, A., van Velthoven, P., ... Bergamaschi, P. (2005). The two-way nested global

chemistry-transport zoom model TM5: algorithm and applications. *Atmospheric Chemistry and Physics*, *5*, 417–432.

/Liang et al, 2017/ Liang, Q., Chipperfield, M. P., Fleming, E. L., Abraham, N. L., Braesicke, P., Burkholder, J. B., … Weiss, R. F.. Deriving global OH abundance and atmospheric lifetimes for long-lived gases: A search for CH3CCl3 alternatives. Journal of Geophysical Research: Atmospheres, 122, 11,914– 11,933. https://doi.org/10.1002/2017JD026926, 2017.

/Louis 1979/ Louis, J.-F. (1979). A parametric model of vertical eddy fluxes in the atmosphere. *Boundary-Layer Meteorology*, *17*(2), 187–202. https://doi.org/10.1007/BF001179788

/Machida et al. 2008/ Machida, T., Matsueda, H., Sawa, Y., Nakagawa, Y., Hirotani, K., Kondo, N., Goto, K., Nakazawa, T., Ishikawa, K., and Ogawa, T.: Worldwide measurements of atmospheric CO_2 and other trace gas species using commercial airlines, J. Atmos. Ocean. Tech., 25(10), 1744–1754, doi:10.1175/2008JTECHA1082.1, 2008.

/Matthews, 1991/ Matthews, E., I. Fung, J. Lerner, Methane emission from rice cultivation: Geographic and seasonal distribution of cultivated areas and emissions, Global Biogeochem. Cycles, 5, 3-24,1991.

/Membrive et al. 2016/ Membrive, O., Crevoisier, C., Sweeney, C., Danis, F., Hertzog, A., Engel, A., Bönisch, H., and Picon, L.: AirCore-HR: A high resolution column sampling to enhance the vertical description of CH_4 and CO_2, Atmos. Meas. Tech. Discuss., doi:10.5194/amt-2016-236, 2016.

/Monteil et al., 2013/ Monteil, G. A., Houweling, S., Butz, A., Guerlet, S., Schepers, D., Hasekamp, O., Frankenberg, C., Scheepmaker, R., Aben, I., & Röckmann, T. (2013). Comparison of CH_4 inversions based on 15 months of GOSAT and SCIAMACHY observations. *Journal of Geophysical Research-Atmospheres*, *118*(20), 11,807–11,823. https://doi.org/10.1002/2013JD019760

/Montzka et al, 2011/ Montzka, S. A., M. Krol, E. J. Dlugokencky, B. Hall, P. Joeckel, J. Lelieveld, Small Interannual Variability of Global Atmospheric Hydroxyl, Science, 331, 67-69, 2011

/NIR-CH, 2019/ NIR-CH, 2019, Switzerland's Greenhouse Gas Inventory 1990–2017, National Inventory Report Including reporting elements under the Kyoto Protocol, www.climatereporting.ch., 2019

/NIR-UK, 2019/ NIR-UK, 2019, UK Greenhouse Gas Inventory, 1990 to 2017, Annual Report for Submission under the Framework Convention on Climate Change. ISBN: 978-0-9933975-5-4, 2019

/Nisbet et al, 2016/ Nisbet, E. G., et al. (2016), Rising atmospheric methane: 2007–2014 growth and isotopic shift, Global Biogeochem. Cycles, 30, 1356–1370, doi:10.1002/2016GB005406.

/Pandey et al., 2019/ Pandy, S., et al., Satellite observations reveal extreme methane leakage from a natural gas well blowout, PNAS, 116 (52) 26376-26381; DOI: 10.1073/pnas.1908712116, 2019.

/Patra et al., 2014/ Patra et al., Observational evidence for interhemispheric hydroxyl-radical parity, Nature volume 513, pages 219–223, doi:10.1038/nature13721, 2014

/Peters et al., 2004/ Peters, W., Krol, M. C., Dlugokencky, E. J., et al.: Toward regional- scale modeling using the two-way nested global model TM5: Characterization of transport using SF_6, J. Geophys. Res., 109, D19314, doi:10.1029/2004JD005020, 2004.

/Pinty et al, 2017/ Pinty B., G. Janssens-Maenhout, M. Dowell, H. Zunker, T. Brunhes, P. Ciais, D. Dee, H. Denier van der Gon, H. Dolman, M. Drinkwater, R. Engelen, M. Heimann, K. Holmlund, R. Husband, A. Kentarchos, Y. Meijer, P. Palmer and M. Scholze An Operational Anthropogenic CO2 Emissions Monitoring & Verification Support capacity - Baseline Requirements, Model Components and Functional Architecture, doi: 10.2760/08644, European Commission Joint Research Centre, EUR 28736 EN, 2017

/README file, 2019/ README file see ReadMe file on www.tropomi.eu /documents/prf

/Prather et al., 1987/ Prather, M. J., McElroy, M. B., Wofsy, S. C., Russell, G., & Rind, D. (1987). Chemistry of the global troposphere: Fluorocarbons as tracers of air motion. *Journal of Geophysical Research*, *92*(D6), 6579–6613.

/Press et al., 2007/ Press, W. H., Teukolsky, S. A., Vetterling, W. T., & Flannery, B. P. (2007). *Numerical Recipes: Vol. New York* (Third). Cambridge University Press.

/Rayner et al., 2019/ Rayner, P., Michalak, A. M., & Chevallier, F. (2016). Fundamentals of Data Assimilation. *Geoscientific Model Development Discussions*, 1–21. https://doi.org/10.5194/gmd-2016-148.

/Reum 2012/ Reum, F. (2012). *Optimization of greenhouse gas flux estimations using data obtained by the GOSAT spacecraft* [PhD Thesis, Friedrich-Schiller-Universität Jena]. http://www.bgc-jena.mpg.de/freum/reum_diploma_thesis.pdf

/Reuter et al., 2013/ Reuter, M., Boesch, H., Bovensmann, H., Bril, A., Buchwitz, M., Butz, A., Burrows, J. P., O'Dell, C. W., Guerlet, S., 730 Hasekamp, O., Heymann, J. , Kikuchi, N., Oshchepkov, S., Parker, R., Pfeifer, S., Schneising, O., Yokota, T., and Yoshida, Y.: A joint effort to deliver satellite retrieved atmospheric CO_2 concentrations for surface flux inversions: the ensemble median algorithm EMMA, Atmos. Chem. Phys., 13, 1771-1780, 2013.

/Reuter et al., 2017/ Reuter, M., M. Buchwitz, O. Schneising, S. Noël, H. Bovensmann, J. P. Burrows, A Fast Atmospheric Trace Gas Retrieval for Hyperspectral Instruments Approximating Multiple Scattering - Part 2: Application to XCO_2 Retrievals from OCO-2, Remote Sens., 9, 1102, doi:10.3390/rs9111102, 2017.

/Reuter et al., 2020/ Reuter, M., Buchwitz, M., Schneising, O., Noel, S., Bovensmann, H., Burrows, J. P., Boesch, H., Di Noia, A., Anand, J., Parker, R. J., Somkuti, P., Wu, L., Hasekamp, O. P., Aben, I., Kuze, A., Suto, H., Shiomi, K., Yoshida, Y., Morino, I., Crisp, D., O'Dell, C., Notholt, J., Petri, C., Warneke, T., Velazco, V., Deutscher, N. M., Griffith, D. W. T., Kivi, R., Pollard, D., Hase, F., Sussmann, R., Te, Y. V., Strong, K., Roche, S., Sha, M. K., De Maziere, M., Feist, D. G., Iraci, L. T., Roehl, C., Retscher, C., and Schepers, D., Ensemble-based satellite-derived carbon dioxide and methane column-averaged dry-air mole fraction data sets (2003-2018) for carbon and climate applications, Atmos. Meas. Tech., 13, 789-819, https://doi.org/10.5194/amt-13-789-2020, 2020.

/Rigby et al., 2017/ Rigby, M., Montzka, S. A., Prinn, R. G., White, J. W. C., Young, D., O'Doherty, S., … Park, S. (2017). Role of atmospheric oxidation in recent methane growth. Proceedings of the National Academy of Sciences, 114(21), 5373–5377. https://doi.org/10.1073/pnas.1616426114

/Rödenbeck 2005/ Rödenbeck, C. (2005). Estimating CO2 sources and sinks from atmospheric mixing ratio measurements using a global inversion of atmospheric transport. *Max-Planck-Institut Fur Biogeochemie*, *TECHNICAL REPORTS 6*, 1–61.

/Rödenbeck et al., 2003/ Rödenbeck, C., Houweling, S., Gloor, M., & Heimann, M. (2003). CO2 flux history 1982–2001 inferred from atmospheric data using a global inversion of atmospheric transport. *Atmospheric Chemistry and Physics*, *3*, 2003.

/Rozanov et al., 2002/ Rozanov, V. V., Buchwitz, M., Eichmann, K.-U., de Beek, R., and Burrows, J. P.: SCIATRAN - a new radiative transfer model for geophysical applications in the 240–2400nm spectral region: The pseudo-spherical version, Adv. Space Res., 29, 1831–1835, 2002.

/Rozanov et al., 2014/ Rozanov, V. V., Rozanov, A. V., Kokhanovsky, A. A., and Burrows, J. P.: Radiative transfer through terrestrial atmosphere and ocean: Software package SCIATRAN, J. Quant. Spectrosc. Radiat. Transfer, 133, 13–71, https://doi.org/10.1016/j.jqsrt.2013.07.004, 2014.

/Russel and Lerner 1981/ Russell, G., & Lerner, J. A. (1981). A New Finite-Differencing Scheme for the Tracer Transport-Equation. *Journal of Applied Meteorology*, *20*(12), 1483–1498.

/Sander et al., 2006/ Sander, S. P., Ravishankara, A. R., Golden, D. M., Kolb, C. E., Kurylo, M. J., Molina, M. J., Moortgart, G. K., Finlayson-Pitts, B. J., Wine, P. H., & Huie, R. E. (2006). *Chemical Kinetics and Photochemical Data for Use in Atmospheric Studies*. Jet Propulsion Laboratory. http://ro.uow.edu.au/scipapers/737/

/Saunois et al, 2016/ Saunois, M., Bousquet, P., Poulter, B., Peregon, A., Ciais, P., Canadell, J. G., … Zhu, Q. (2016). The global methane budget 2000-2012. Earth System Science Data, 8(2), 697–751. https://doi.org/10.5194/essd-8-697-2016.

/Schaefer et al, 2016/ Schaefer, H., Fletcher, S. E. M., Veidt, C., Lassey, K. R., Brailsford, G. W., Bromley, T. M., … White, J. W. C. (2016). A 21st-century shift from

fossil-fuel to biogenic methane emissions indicated by 13CH4, Science, 352, 6281, pp 80-84.

/Schepers et al., 2012/ Schepers, D., Guerlet, S., Butz, A., Landgraf, J., Frankenberg, C., Hasekamp, O., ... Aben, I. (2012). Methane retrievals from Greenhouse Gases Observing Satellite (GOSAT) shortwave infrared measurements: Performance comparison of proxy and physics retrieval algorithms. *Journal of Geophysical Research: Atmospheres*, *117*(D10), doi: 10.1029/2012JD017549.

/Schneising et al., 2019a/ Schneising, O., Buchwitz, M., Reuter, M., Bovensmann, H., Burrows, J. P., Borsdorff, T., Deutscher, N. M., Feist, D. G., Griffith, D. W. T., Hase, F., Hermans, C., Iraci, L. T., Kivi, R., Landgraf, J., Morino, I., Notholt, J., Petri, C., Pollard, D. F., Roche, S., Shiomi, K., Strong, K., Sussmann, R., Velazco, V. A., Warneke, T., and Wunch, D.: A scientific algorithm to simultaneously retrieve carbon monoxide and methane from TROPOMI onboard Sentinel-5 Precursor, Atmos. Meas. Tech., 12, 6771-6802, https://doi.org/10.5194/amt-12-6771-2019, https://doi.org/10.5194/amt-12-6771-2019, 2019.

/Schneising et al., 2019b/ Schneising, O., et al., ESA Climate Change Initiative "Plus" (CCI+) Algorithm Theoretical Basis Document (ATBD) - TROPOMI WFM-DOAS XCH_4, technical report ESA project GHG-CCI+, version 1, 20-August-2020, pp. 25, 2019.

/Scott and Chédin, 1981/ Scott, N.A. and Chédin, A., A Fast Line-by-Line Method for Atmospheric Absorption Computations: The Automatized Atmospheric Absorption Atlas. J. Appl. Meteorol. 20, 802–812. doi:10.1175/1520-0450(1981)020<0802:AFLBLM>2.0.CO;2, 1981.

/Segers and Houweling, 2018/ Segers, A. and S. Houweling, 2018, Description of the CH4 Inversion Production Chain, Copernicus Atmosphere Monitoring Service, https://atmosphere.copernicus.eu/sites/default/files/2018-12/CAMS73_2015SC3_D73.2.5.5-2018_201811_production_chain_update_v2.pdf, 2018.

/Segers and Houweling, 2020/ Segers, A. and S. Houweling, 2020, Description of the CH4 Inversion Production Chain, Copernicus Atmosphere Monitoring Service,

https://atmosphere.copernicus.eu/sites/default/files/2020-01/CAMS73_2018SC1_D73.5.2.2-2019_202001_production_chain_v1.pdf

/Shindell et al, 2017/ Shindell, D. T., Fuglestvedt, J. S., Collins, W. J., The social cost of methane: theory and applications, Faraday Discussions, 200, 429-451, DOI: 10.1039/c7fd00009j, 2017.

/Siddans et al., 2017/ Siddans R., Knappett, D., Kerridge, B., Waterfall, A., Hurley, J., Latter, B., Boesch, H., and Parker, R., Global height-resolved methane retrievals from the Infrared Atmospheric Sounding Interferometer (IASI) on MetOp, Atmos. Meas. Tech., 10, 4135-4164, http://doi.org/10.5194/amt-10-4135-2017, 2017.

/Siddans, 2019/ Siddans R., IMS ATBD, Water Vapour Climate Change Initiative (WV_cci), D2.2, CCIWV.REP.005, 2019.

/Tiedke 1989/ Tiedke, M. A Comprehensive Mass Flux Scheme for Cumulus Parameterization in Large Scale Models. *Bulletin of the American Meteorological Society*, *117*, 1779–1799, 1989.

Turner et al, 2016/ Turner, A. J., Maasakkers, J. D., Sheng, J., Sun, K., Liu, X., Chance, K., Aben, I., McKeever, J., and Frankenberg, C.: Satellite observations of atmospheric methane and their value for quantifying methane emissions, Atmos. Chem. Phys., 16, 14371-14396, https://doi-org.vu-nl.idm.oclc.org/10.5194/acp-16-14371-2016, 2016.

/Varon et al., 2019/ Varon, D. J., McKeever, J., Jervis, D., Maasakkers, J. D., Pandey, S., Houweling, S., et al., Satellite discovery of anomalously large methane point sources from oil/gas production. Geophysical Research Letters, 46, 13,507–13,516. https://doi.org/10.1029/2019GL083798, 2019.

/Veefkind et al., 2012/ Veefkind, Aben, et al., TROPOMI on the ESA Sentinel-5 Precursor : a GMES mission fro global observations of the atmospheric composition for climate, air quality and ozone layer applications, Remote Sensing Environment, doi:10.1016/j.rse.2011.09.027, 2012.

/Worden et al, 2015/ Worden, J. R., Turner, A. J., Bloom, A., Kulawik, S. S., Liu, J., Lee, M., Weidner, R., Bowman, K., Frankenberg, C., Parker, R., and Payne, V. H.: Quantifying lower tropospheric methane concentrations using GOSAT near-IR and TES thermal IR measurements, Atmos. Meas. Tech., 8, 3433-3445, https://doi.org/10.5194/amt-8-3433-2015, 2015.

/Worden et al, 2017/ Worden, J. R., Bloom, A. A., Pandey, S., Jiang, Z., Worden, H. M., Walker, T. W., Houweling, S., and Röckmann, T.: Reduced biomass burning emissions reconcile conflicting estimates of the post-2006 atmospheric methane budget, Nature Communications, 8, 2227, doi:10.1038/s41467-017-02246-0, 2017.

/Wunch et al, 2010/ Wunch, D., et al., Calibration of the TCCON using aircraft profile data, Atmos.meas.Tech., 3, 1351-1362, doi:10.5194/amt-3-1351-2010, 2010.

/Wunch et al. 2011/ Wunch, D., Toon, G. C., Blavier, J.-F. L., Washenfelder, R. A., Notholt, J., Connor, B. J., Griffith, D. W. T., Sherlock, V., 845 and Wennberg, P. O.: The Total Carbon Column Observing Network. Phil. Trans. R. Soc. A, 369, 2087–2112, doi:10.1098/rsta.2010.0240, 2011.

/Yurganov and Leifer/ Yurganov L.N., & Leifer I., 2016. Anomal'nye kontsentratsii atmosfernogo metana nad Okhotskim morem zimoi 2015/2016 g.g.(Abnormal concentrations of atmospheric methane over the Sea of Okhotsk during 2015/2016 winter). Sovremennye problemy distantsionnogo zondirovaniya zemli iz kosmosa 13(3), 231-234.

/Xiong et al., 2009/ Xiong, X., Houweling, S., Wei, J., Maddy, E., Sun, F., and Barnet, C., 2009: Methane plume over south Asia during the monsoon season: satellite observation and model simulation, Atmos. Chem. Phys., 9, 783-794, doi:10.5194/acp-9-783-2009.

/Xiong et al., 2010/ Xiong, X., et al., 2010: Mid-upper tropospheric methane in the high Northern Hemisphere: Spaceborne observations by AIRS, aircraft measurements, and model simulations, Journal of Geophysical Research: Atmospheres, 115, D19309, doi: 10.1029/2009jd013796.

/Zhang et al. 2018/ Zhang, Zhen, Niklaus E Zimmermann, Leonardo Calle, George Hurtt, Abhishek Chatterjee, and Benjamin Poulter (2018). Enhanced Response of Global Wetland Methane Emissions to the 2015-2016 El Nino-Southern Oscillation Event. Environmental Research Letters 13 (5), 074009. doi: 10.1088/1748-9326/aac939.

***** End of Document *****